Departamento de Ingeniería Biomédica

TRABAJO FIN DE GRADO

DYNAMIC CONTRAST IMAGING: PROTOCOL OPTIMIZATION

Autor: María Gómez de Salazar Cordero

Director: Paula Montesinos Suárez de la Vega

Co-Director: Lorena Cussó Mula

Leganés, 9 de julio de 2014

Título: Dynamic Contrast Imaging: Protocol Optimization
Autor: María Gómez de Salazar Cordero
Director: Paula Montesinos Suárez de la Vega
Co-director: Lorena Cussó Mula

EL TRIBUNAL

Presidente:

Vocal:

Secretario:

Realizado el acto de defensa y lectura del Trabajo Fin de Grado el día 9 de julio de 2014, en la Escuela Politécnica Superior de la Universidad Carlos III de Madrid, acuerda otorgarle la CALIFICACIÓN de:

VOCAL

SECRETARIO PRESIDENTE

Agradecimientos

En este punto, me gustaría dar las gracias a Dios por todas las personas que han contribuido directa o indirectamente en este trabajo.

En primer lugar quiero dar las gracias al Laboratorio de Imagen Médica del Hospital Gregorio Marañón por haberme dejado realizar este proyecto con ellos. A mis guías durante todo este tiempo Lorena Cussó y Paula Montesinos por su total disponibilidad, siempre dispuestas a solucionar mis dudas, a compartir sus conocimientos y a cuidarme. Sin vosotras nada de esto habría sido posible.

A mis compañeros del "buffer", en especial a Pedro por su infinita paciencia y por haberme ayudado siempre que lo he necesitado; y a Iván por dibujarme una sonrisa todos los días. A todos mis compañeros del LIM siempre dispuestos a animar a sus "proyectandos".

A mis amigos y compañeros de universidad. A mis amigos de toda la vida.

A mi familia, sin la cual no habría llegado hasta aquí. Muchas gracias por animarme, por vigilarme y por quitarle hierro al asunto. A Lourditas, por ser la única capaz de alegrarme el día sin decir una palabra. Y especialmente a mi madre, siempre dispuesta a todo por mí, por haber venido siempre que lo he necesitado, por sus consejos, por todo.

A todos vosotros, muchísimas gracias.

El presente proyecto ha sido realizado en la Unidad de Medicina y Cirugía Experimental del Hospital General Universitario Gregorio Marañón, bajo la dirección de Paula Montesinos Suárez de la Vega y Lorena Cussó Mula

Abstract

Cancer is one of the principal leading causes of death worldwide, and thus it is one of the most studied diseases. Animal models have been used during centuries to increase human knowledge of these and other diseases. Magnetic Resonance Imaging (MRI) is one of most commonly used techniques to retrieve non-invasively anatomical and functional information of tumors. Several works have defined the perfusion grade as an advantageous indicator for the design of new cancer therapies.

In this context, it comes up the project presented in this document. Due to the variety of protocols find in the literature to study tumor perfusion, the purpose of this project is the optimization of two Dynamic Magnetic Resonance Imaging (DMRI) protocols (for Dynamic Contrast Enhanced-MRI (DCE-MRI) and Dynamic Susceptibility Contrast MRI (DSC-MRI) techniques respectively) to evaluate pancreatic tumor perfusion in nude mice. To do that, different DMRI sequences with an administered contrast agent were tested. For the optimization of the DCE-MRI two different contrast agent doses were tested. And to optimize DSC-MRI protocol two contrast media volumes were tested.

For the evaluation and analysis of the dynamic images obtained three image processing programs were employed. One of them was used to evaluate the quality of the images obtained. And the other two were employed to obtain quantitative parameters of the dynamic images.

Keywords: MRI, tumor, DMRI, DCE-MRI, DSC-MRI, contrast agent.

Index

1.Motivation and Objectives 1
1.1 Motivation 1
1.2 Objectives 2
2.Introduction 4
2.1 MRI physical principles 5
2.1.1 Relaxation process 7
2.2 Dynamic contrast MRI principles 9
2.2.1 Contrast relaxation agents 10
2.2.2 DCE-MRI: T1 relaxation 11
2.2.3 DSC-MRI: T2* relaxation 12
2.2.4 Dynamic imaging in tumors 12
2.3 Data quantification 15
2.3.1 DCE-MRI quantification 15
2.3.2 DSC-MRI quantification 18
3.Materials and Methods 21
3.1 Animals 21
3.1.1 Animal preparation 22
3.2 Image acquisition 23
3.2.1 DCE-MRI acquisition 25
3.2.2 DSC-MRI acquisition 25
3.3 Image processing 26
3.3.1 DCE-MRI analysis 27
3.3.2 DSC-MRI analysis 29
4.Results 32

4.1 DCE-MRI optimization 32
4.2 DSC-MRI optimization..... 36
4.3 Quantitative analysis..... 39
4.3.1 DCE-MRI quantification..... 39
4.3.2 DSC-MRI quantification..... 42
5.Discussion..... 46
5.1 DCE-MRI optimization 47
5.2 DSC-MRI optimization..... 47
5.3 DCE and DSC: comparative 48
6.Conclusions and future perspectives 51
6.1 Conclusions..... 51
6.2 Future perspectives 52

Figure Index

Figure 1. Schematic representation of signal detection [9]. 6

Figure 2 Magnetic resonance images weighted in T1 A), and T2 B) [1]. 8

Figure 3. Time intensity curve after the administration of a contrast agent in a patient with breast cancer [8]. 9

Figure 4. Comparison of the T1-weighted DCE-MRI (top) and T2-wieghted DSC-MRI (bottom) data collections from a patient with a prostate tumor, by the administration of Gd-DTPA [26]. 14

Figure 5. Schematic representation of the Hoffman model. 17

Figure 6. Anesthesia system (A) and position of the mouse (B). 22

Figure 7. Instrumentation employed for the MR images acquisition. A) Injection pump.. B) Programmable part of the injection pump. C) 7T MRI system where the black arrows point at the warm water system, the green at the rectal temperature motorization, and the red arrow point at the breathing rate monitor. 23

Figure 8. Diagram showing the imaging protocol for the DMRI images acquisition. ... 24

Figure 9. Process followed to quantify DCE images with DCE@urLAB software. Step 1 the software is opened, image imported and injection frame defined. Step 2 the ROI (tumor) is defined manually. Step 3 and 4 pharmacokinetic analysis of Hoffman model. Step 3’ and 4’ semi-quantitative analysis using the curve parameters model. 27

Figure 10. Dynamic image (A) with a ROI defined, and relative contrast enhancement image (B) represented with DCE@urLAB software. 28

Figure 11. RCE images with different Min and Max values for the color scale. 29

Figure 12. Order followed to analyze DSC-MRI data. Step 1 images imported to ImageJ. Step 2 LIM perfusion plugin is opened. Then, AIF is calculated semi-manually (step 3).Finally, parametric maps are obtained (step 4). 29

Figure 13. Process to select a good AIF. A) Image analyzed, where the red arrow points at the aorta, region where the AIF should be selected. B) Top, example of a right AIF; bottom, example of a wrong AIF..... 30

Figure 14. DCE-MRI images acquired before (A) and after (B) the contrast agent administration; contrast dose and volume: 0.1 mmol/kg body weight in 0.2 ml. The white arrow points the tumor localization. 32

Figure 15. DCE-MRI images acquired before (A) and after (B) the contrast agent administration using the Fire option of ImageJ, contrast dose and volume: 0.1 mmol/kg body weight in 0.2 ml. 33

Figure 16. Dynamic Pixel Inspector analysis of DCE-MRI images with a Gadovist dose of 0.1 mmol/kg body weight diluted in 0.2 ml. 34

Figure 17. DCE-MRI images acquired before (A) and after (B) the contrast agent administration; contrast dose and volume: 0.05 mmol/kg body weight in 0.12 ml. The white arrow points the tumor localization. 34

Figure 18. DCE-MRI images acquired before (A) and after (B) the contrast agent administration using the Fire option of ImageJ. Gadovist dose 0.05 mmol/kg body weight, and diluted in 0.12 ml. 35

Figure 19. Dynamic Pixel Inspector analysis of DCE-MRI images with a Gadovist dose of 0.05 mmol/kg body weight diluted in 0.12 ml. 35

Figure 20. DSC-MRI images acquired before (A) and after (B) the contrast agent administration; contrast agent volume 0.12 ml. The white arrow points the tumor localization..... 36

Figure 21. DSC-MRI images acquired before (pre-contrast image; A) and after (post-contrast image; B) the contrast agent administration using the Fire option of ImageJ. Contrast agent volume 0.12 ml. 36

Figure 22. Dynamic Pixel Inspector analysis of DSC-MRI images with a contrast media of 0.12 ml..... 37

Figure 23. DSC-MRI images acquired before (pre-contrast image; A) and after (post-contrast image; B) the contrast agent administration; contrast agent volume 0.2 ml. The white arrow points the tumor localization. 37

Figure 24. DSC-MRI images acquired before (pre-contrast image; A) and after (post-contrast image; B) the contrast agent administration using the Fire option of ImageJ. Contrast agent volume 0.2 ml. 38

Figure 25. Dynamic Pixel Inspector analysis of DSC-MRI images with a contrast media of 0.2 ml..... 38

Figure 26. Original DCE-MRI image with the ROI selected for the quantification analysis. 39

Figure 27. Pharmacokinetic parameters of the Hoffman model in the ROI (tumor) of DCE-MRI images. A) A.kep; B) kep; C) A^H; and D) kel 40

Figure 28. Parameters of the curve parameters model in the ROI (tumor) of DCE-MRI images. A) IAUC; B) RCE; and C) TTM..... 41

Figure 29. DSC-MRI images acquired before (pre-contrast image; A) and after (post-contrast image; B) the contrast agent administration; contrast agent volume 0.2 ml.. 42

Figure 30. BV parametric map represented in two color scales. A) Grays. B) MMWKS program (red-blue color scheme). 43

Figure 31. BF parametric map represented in different color scales. A) Grays. B) MMWKS program (red-blue color scheme). 43

Figure 32. MTT parametric map represented in the gray scale (A), and in the red-blue color scheme acquired with the MMWKS (B)..... 44

Acronyms

Arrange by ordered of appearance

CNIO: Centro Nacional de Investigaciones Oncológicas

MNP: Magnetic Nano-Particles

MRI: Magnetic Resonance Imaging

DMRI: Dynamic MRI

PET: Positron Emission Tomography

CT: Computed Tomography

SPECT: Single Photon Emission Computed Tomography

MR: Magnetic Resonance

RF: Resonance Frequency

GRE: Gradient-Echo

SE: Spin-Echo

ADC: Analog-to-Digital Converter

T1-w: T1-weighted

T2*-w: T2*-weighted

TIC: Time Intensity Curve

DCE: Dynamic Contrast Enhanced

DSC: Dynamic Susceptibility Contrast

EES: Extravascular Extracellular Space

VEGF: Vascular Endothelial Growth Factors

IAUC: Initial Area Under the Curve

RCE: Relative Contrast Enhancement

TTM: Time To Maximum enhancement

TAC: Time Activity Curve

AIF: Arterial Input Function

BV: Blood Volume

BF: Blood Flow

MTT: Mean Transit Time

FoV: Field of View

FLASH: Fast Low Angle Shot

TR: Repetition Time

NA: Number of Averages

MMWKS: Multimodality WorkStation

ETSIT: Escuela Técnica Superior de Ingenieros de Telecomunicaciones

ROI: Region Of Interest

RR: Reference Region

rBV: relative Blood Volume

rBF: relative Blood Flow

Outline of the document

The present document is organized in 6 chapters. Chapter 1 presents the motivations of this project, and its main objectives. In chapter 2 a brief introduction of the MRI physical principles is exposed and also a description about how these images can be acquired and processed. Chapter 3 presents the protocols selected and the programs employed for the quantification of the images. In chapter 4 the results obtained with the image acquisition protocols and the parameters calculated with the software programs are exposed objectively. Chapter 5 presents the discussion of the results shown in the previous chapter. Finally, in chapter 6 the conclusions of the project and its future perspectives are exposed.

Chapter 1

Motivation and Objectives

1.1 Motivation

Cancer is one of the principal leading causes of death worldwide, and thus one of the most studied diseases. To study this and other diseases animal models have been used during centuries; in order to increase human knowledge of normal and malfunctioning cells, to improve efficacy of chemical compounds for therapy, to test new interventional techniques, etc. Animal models allow researchers to discover the underlying basis of how and why cancer arise, why primary tumors metastasize, and how various kinds of preventive interventions and treatments can be used to stop the progress, growth and spread of tumors, and prolong patient lives. Research with animal models using imaging and other diagnostic techniques can help in the definition of new treatment strategies [1].

Several works have defined the perfusion grade as an advantageous indicator for the design of new cancer therapies, or to develop new studies. A tumor highly perfused is synonym of a tumor highly vascularized, and the higher the vascularization, the higher the tumor grade (aggressiveness) [2].

In this context, it comes up the project “MRI study of tumor vascularization and delivery of magnetic nanoparticles” developed by the Unidad de Medicina y Cirugía Experimental of the Hospital General Universitario Gregorio Marañón in collaboration with the Stem Cells & Cancer Group of the Centro Nacional de Investigaciones Oncológicas (CNIO). The main goal of this project is to deliver multifunctionalised magnetic nanoparticles (MNP) in a nude mouse with different types of pancreatic tumors implanted (xenograft). These MNP will selectively target to destroy pancreatic cancer cells.

In the mentioned project, the MNP will be tested in different tumors with different perfusion grades, Magnetic Resonance Imaging (MRI) will be used to evaluate the perfusion of those tumors, and thus the selection and optimization of an MRI protocol with that purpose is required.

There exists an extended and varied literature about MRI protocols to evaluate tumor perfusion by using Dynamic Magnetic Resonance Imaging (DMRI), which involves the serial acquisition of images during the injection of a contrast agent. However, the technique is complex and it is not completely established. Therefore, the necessity to determine the optimum protocol for this study. There are two main approaches to evaluate DMRI: DCE-MRI and DSC-MRI, both approaches are evaluated in this work.

1.2 Objectives

The main goal of this project is to determine the optimum protocol of DMRI to study the perfusion grade of subcutaneous 215 pancreatic tumors. To do that, both DCE-MRI and DSC-MRI approaches and different contrast agent concentrations will be tested and compared.

Chapter 2

Introduction

The term molecular imaging refers to the set of imaging techniques and processes used to produce non-invasive images from inside the body, that give information about the structure and the function of these inside parts to help in the detection of possible anomalies [3, 4]. These medical imaging modalities are able to detect cellular processes at molecular level in vivo, without perturbing the biological system studied.

Molecular imaging techniques allow to develop imaging systems highly sensitive, specific and with amplification methods for complex situations where sensitivity is low [3]. The information that these techniques can offer, allows physicians to create a more personalized treatment planning for the patient [5].

In a general way, molecular imaging techniques are based on systems able to detect different physical signals emitted by some biological molecules that are imperceptible for humans. Once these signals are detected, the system converts them in data that is digitalized, and allows the formation of an image. Depending on the imaging technique, the information obtained could be structural, functional or both [6].

These imaging techniques can be classified according to the type of signal used to create the images: techniques based on the employment of ionizing radiation such as X-rays,

positron emission tomography (PET), computed tomography (CT), scintigraphy (two-dimensional images) and single photon-emission computed tomography (SPECT); and techniques that used non-ionizing radiation like MRI, ultrasound and optical imaging [5].

Both SPECT and PET are nuclear imaging techniques highly used in clinical for the diagnoses of multiple pathologies such as infection (by nuclear labeled leucocytes), cancer and myocardial infarct (by Fludeoxyglucose metabolism). Nowadays, due to their high sensitivity nuclear imaging is extensively used in preclinical research. However, in preclinical settings PET is more employed than SPECT because of its higher sensitivity and spatial and temporal resolution. Another imaging technique widely employed in clinical and preclinical research is CT; this technique is characterized by its high spatial and temporal resolution, contributing to medicine by offering a volumetric representation of the body with high diagnostic value. Optical imaging is highly extended in biomedical research for in vitro and ex vivo studies due to its simplicity and low cost. Finally, MRI technique is able to obtain anatomical, functional and even chemical information of the subject study. Besides its good spatial resolution (as CT), MRI provides better contrast in soft tissues than other modalities [4].

The different types of images that can be acquired with MRI and its excellent properties (high spatial and temporal resolution, non-ionizing signal, etc) make it one of the most value tools for the diagnostic of tumor lesions in the musculoskeletal system. It is a technique that can be used either for the study of anatomical structures or for the physiological knowledge [7-9].

2.1 MRI physical principles

Magnetic Resonance (MR) effect was discovered in 1929 by the physician Isidor Isaac Rabi [10]; and since its discovery it has continued growing day a day.

MRI is a complex technique based on the physical phenomenon named nuclear magnetic resonance. In general terms, it can be defined as a phenomenon in which

certain atomic nucleus (those with non-zero spin values) are able to absorb and emit electromagnetic energy at a specific frequency (Larmor frequency) in presence of a magnetic field [9].

Although several nuclei can be studied with this technique, the most studied one is the hydrogen (^{1}H), as ^{1}H is the most abundant elements in nature and in the human body. That is the reason why sometimes MRI literature is referred to protons or spins instead of nuclei.

MRI acquisition is a set of processes where the sample of interest is exposed to an external static magnetic field and it is excited with an oscillating magnetic field at a specific frequency corresponding to the resonance frequency of the nuclei (RF). The RF energy is absorbed by the sample, and after excitation the sample relax emitting RF energy, this energy is recorded by a coil. This coil obtains the MR signal that ultimately will form the MR images [11].

As it can be observed in Figure 1 the MRI signal is a continuous signal; this signal is measured and recorded using an analog-to-digital converter (ADC). Once the signal is digitized, the MR image can be obtained. The explanation of the details of MRI technique is beyond the scope of this project, for further details about MRI physical principles the following books can be consulted [9, 12].

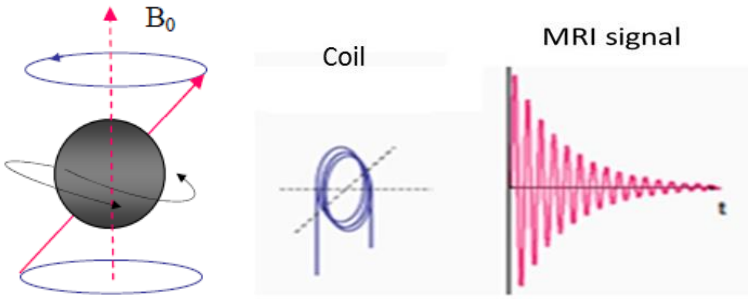

Figure 1. Schematic representation of signal detection [9].

An image to be formed requires more than a single MR signal; thus, it requires more than a RF excitation, so, the application of a sequence of different RF pulses and magnetic field gradients is needed. This process is known as MRI sequences [9, 13-15].

There exist multiple types of MRI sequences. Some of the most employed are spin-echo (SE), inversion recovery (IR) and gradient-echo (GRE) sequences. Depending on the image conditions a sequence or another will be used.

2.1.1 Relaxation process

The process by which nuclei emit the energy absorbed is known as relaxation process. This relaxation process is the base for tissue contrast in MRI. Two different relaxation processes can be measured in magnetic resonance techniques: T1 and T2.

- Relaxation T1, also known as spin-lattice relaxation time, is the mechanism by which nuclei give up their energy to the surrounding. T1 is defined as a constant of time which characterized this process [9, 16]. T1 constant depends on many factors, such as the size of molecules of the sample, the nature of those molecules, and the existence of macromolecules in the lattice. The molecular motion of nuclei (rotational, translational and vibrational) also influences T1 value, affecting to the facility (those with short T1 values) or difficulty (large T1 values) nuclei have to release their energy [17]. Therefore, T1 is an intrinsic property of each tissue, and it produces different intensities in the image for different tissues.

  Those differences in the T1 of tissues can be exploited by applying a T1 weighted (T1-w) sequence in MRI [9]. Figure 2A shows an example of a T1-w image of a human brain.

- Relaxation T2, also named spin-spin relaxation time, refers to the energy transfer from an excited nucleus to another nearby nucleus. This process is characterized by the T2 constant [9, 16]. T2 also depends on the nature of molecules of the sample, and on its surrounding molecules. Thus, it also can be considered as an intrinsic property of each tissue that will affect the facility (short T2 values) or difficulty (large T2 values) to decay. As in T1 relaxation time, these differences in magnitude will create an image where different tissues will present different intensities and thus can be differentiated [9].

As in T1, a T2 weighted (T2-w) sequence can be applied to T2 to enhance the differences in the T2 of tissues [9]. An example of a T2-w image can be observed in Figure 2B.

In an idealized system, T2 relaxation will be affected only by the nature of the nuclei. However, in real systems there are small inhomogeneities originated by the magnetic field and also by the spin-spin interactions that will also affect T2 relaxation. Thus, the real spin-spin relaxation time constant is named T2*, a constant that considers both the T2 value of tissue and the effects of the magnetic field inhomogeneities

$$\frac{1}{T_2^*} = \frac{1}{T_2} + \frac{1}{T_{inhom}} \qquad (2.1)$$

Every tissue in human body has its own T1 and T2 values; an example is presented in Figure 2, where those intensity differences mentioned before can be observed. In the image weighted in T1 (T1-w), tissues with high T1 values, such as cerebrospinal fluid, will have lower intensity and will appear darker; and tissues with low T1 values like fat will have higher intensity and will appear brighter. While in the T2-w image, tissues with high T2 values, such as cerebrospinal fluid, will be represented brighter; and those with low T2 values like fat or gray matter will appear darker.

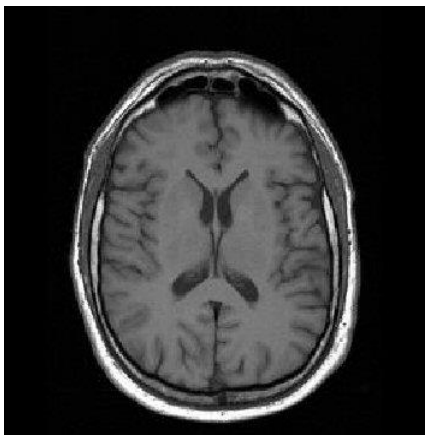

A)

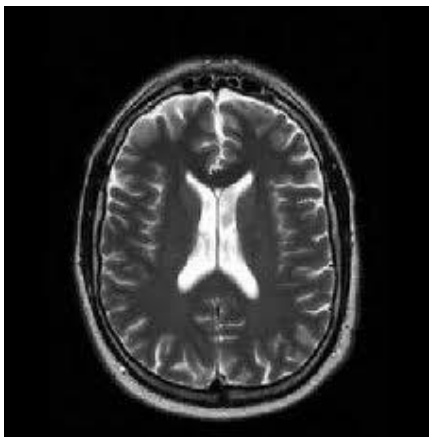

B)

Figure 2 Magnetic resonance images weighted in T1 A), and T2 B) [1].

2.2 Dynamic contrast MRI principles

The different tissue intensities that MRI offers, allow physicians to diagnose pathologic tissues, based on the different relaxation times of healthy and disease tissues. These signal differences between normal and pathologic tissue can be enhanced by the intravenous administration of a contrast agent.

Moreover, the employment of a contrast agent with DMRI sequence allows the knowledge of the physiology of the sample studied. DMRI involves the serial acquisition of images before, during and after the injection of a contrast agent. As the contrast agent enters the region under study, it changes T1, T2 or both; and thereby alters the MR signal intensity [18]. This fact also enables the tracking of the contrast media injected.

DMRI sequences are highly advantageous tools for tumor diagnostic in the musculoskeletal system. The tracking of the contrast agent informs about the physiological contrast distribution, which is defined in a time intensity curve (TIC). This TIC shows the effect of the contrast in the relaxation times while it passes through the vessels (Figure 3). Therefore, a high temporal resolution is required to visualize these changes. The analysis of the contrast distribution enables the knowledge of tumor vascularization, tissue perfusion and capillary permeability [2, 19].

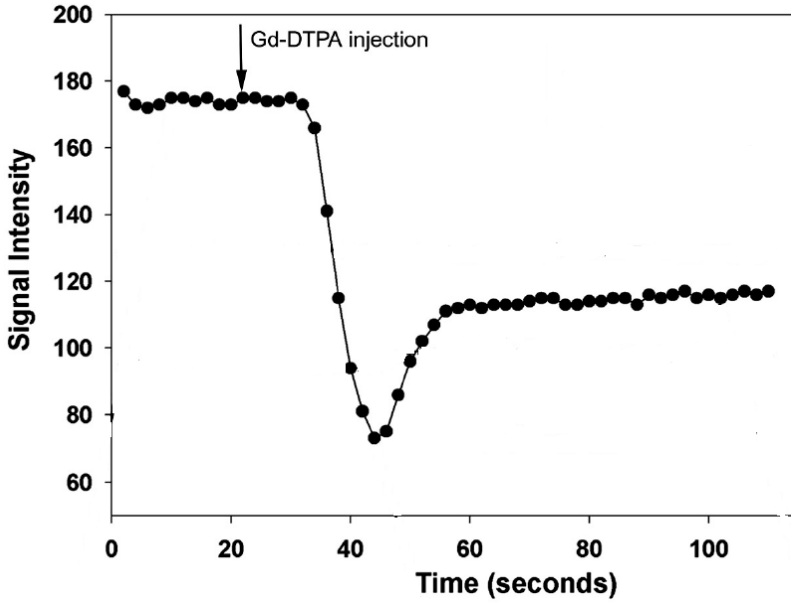

Figure 3. Time intensity curve after the administration of a contrast agent in a patient with breast cancer [8].

There are two different types of dynamic MR sequences: dynamic-contrast-enhanced MRI (DCE-MRI) and dynamic-susceptibility-contrast MRI (DSC-MRI). DCE-MRI is performed with T1-w images, and DSC-MRI with T2*-w images.

To obtain dynamic images different MR sequences can be applied (spin-echo, VIBE, gradient echo, etc). However, for the analysis of tumor perfusion required in this project a gradient echo sequence was selected. This type of sequence is characterized by its high sensitivity and its fast MR signal acquisition [8]. Both characteristics are essential for tracking the contrast agent to study the tumor perfusion.

2.2.1 Contrast relaxation agents

As it has been mentioned before, signal differences among tissues can be enhanced by the administration of a contrast agent.

MRI contrast agents are chemical compounds that affect the relaxation times of the nuclei presented in the tissue [20], and those relaxation time differences produce changes in the intensities between the tissues of the sample.

The ability of a contrast agent to enhance the nucleus relaxation rate is defined in terms of its relaxivity,

$$R_{1,2} = R_{1,2}^{0} + r_{1,2}C \qquad (2.2)$$

Where $R_{1,2}^{0}$ are the relaxation rates (R_1, R_2) without the presence of the contrast agent, C is the concentration (molar) of the contrast agent and $r_{1,2}$ are the relaxivity constants (T1 and T2) of the agent [21]

Based on their effect of shortening the T1 or T2 constants, MRI agents can be categorized as T1 or T2 contrast agents [20].

- T1 relaxation agents are formed by one or more paramagnetic metal ions that contain one or more unpaired electrons. Its main function is the shortening of T1 relaxation time of the tissues affected by it, making them to become brighter (higher signal).

- T2 relaxation agents are typically formed by an agglomerate of iron atoms that collectively formed a superparamagnetic center. The use of these agents results in a shortening of T2 relaxation time of the tissues. This shortening of T2 affects to the signal intensity making it lower, and thus, the image will become darker.

However, there exists some contrast agents that affects both T1 and T2 relaxation times. Some of the most employed ones are based on Gadolinium. In general these contrast agents are strongly paramagnetic, stable, effective and low-molecular weight complexes. Gadolinium contains seven unpaired electrons and is able to reduce MRI relaxation processes producing a decrease in T1 and T2. Thus, it can be used in both DCE-MRI and DSC-MRI. Contrast media with Gadolinium has shown no short-term toxicity, making it optimal for clinical researches [22]. Therefore, it is an advantageous contrast agent since it can be translated without problem from preclinical to clinical studies.

2.2.2 DCE-MRI: T1 relaxation

DCE-MRI is a dynamic technique able to exploit T1 changes caused by the administration of a contrast agent. It allows the measurement of permeability and perfusion by acquiring images before, during and after the administration of a contrast agent. The degree of signal enhancement seen on T1-w is dependent on many factors; some of them include tissue perfusion, capillary permeability, the native T1 relaxation rates of the tissue and the contrast agent dose [8].

With this technique, it can be observed the passage of the contrast media intravascularly and its leakage in the extravascular space. DCE-MRI is sensitive to the presence of contrast medium both within vessels and in the extravascular extracellular space (EES) [23, 24]. Besides the intensity changes produced in the blood vessels, in tumors, typically 12-45% of the contrast media leaks into the EES during the first pass of the contrast [25], this percentage leakage allows to change tumor region relaxation time and thus it permits its visualization with a different signal intensity. Once out of the blood vessels the contrast agent is free to diffuse within the interstitial space until whole body distribution and renal excretion lowers the contrast concentration.

2.2.3 DSC-MRI: T2* relaxation

The second dynamic MRI technique is the DSC-MRI or perfusion-weighted. As DCE-MRI sequences, DSC-MRI permits to study permeability and perfusion of a certain region by continuous acquisition of images before, during and after the injection of a contrast agent. In DSC-MRI the changes caused by the contrast agent in T2 relaxation are exploited. The degree of signal loss observed is dependent on the vascular concentration of the contrast agent and also on the microvessel size and its density [8].

The contrast mechanism of this imaging technique is based on the magnetic susceptibility properties of the contrast agent that creates local field inhomogeneities and thus changes in the T2* relaxation times. The contrast agent leaks through the vessel walls into the interstitium, achieving intravascular contrast agent concentration high enough to produce variations of the T2* relaxation time and thus to the signal intensity of the tissue [23, 26].

2.2.4 Dynamic imaging in tumors

It has been highlighted the study of tumor vascularity to know the aggressiveness of the tumor [2, 27]. For these studies different techniques can be employed, such as biopsies and vascular endothelial growth factors (VEGF). However, these methodologies have some drawbacks like the lack of sensitivity (VEGF) and the surgical invasion (biopsy) [23].

Alternatively, some imaging modalities such as MRI, can be used for studying tumor structure and physiology in a non-invasively and repeatedly manner. Some of these techniques are DCE-MRI and DSC-MRI. DCE-MRI enables to study tumor vasculature by measuring perfusion, vascular permeability and blood volume. While DSC-MRI allows to measure the blood flow and the blood volume [8, 23].

Both DMRI techniques differ in their characteristics; some of the most noticeable are the phase of the contrast passage studied, or the temporal resolution. DCE-MRI studies the contrast passage in both vascular and extravascular space. While, DSC-MRI just interrogate the vascular space. Moreover, DCE-MRI possesses a temporal resolution of the order of 2-25 seconds. Whilst, DSC-MRI has a temporal resolution of 1-2 seconds

for an optimal data acquisition. Although DSC-MRI possesses some limitations, it is able to quantify microvasculature changes due to its rapid imaging acquisition [28], and the image acquisition follows a relatively simple protocol. Even though DCE-MRI requires a more complicated protocol, and it is not able to quantify those microvasculature changes since it requires a larger time to carry out an optimal image acquisition [8, 26]. A summary of the differences of these and other characteristics of both DMRI sequences is presented in Table 1.

Although both of them are able to evaluate tumors, present literature is contradictory. Some authors have categorized DCE-MRI as the general dynamic technique to study tumors in regions outside the brain, such as the heart, breast, prostate, etc [29-32]. While DSC-MRI has been defined as the standard dynamic technique to study intracranial tumors [33, 34]. These classifications have been done because DSC-MRI is more difficult to implement when studying extracranial tissues, such as pelvis, due to field inhomogeneity effects, and the fact that DSC-MRI standard analysis does not take into account extravasation [35].

	DSC- MRI	DCE-MRI
Mechanism of tissue enhancement	Susceptibility effects of contrast agent on magnetic field	Relaxivity effects of contrasts agent on tissue water
Tissue compartment being interrogated	Vascular space	Vascular and extravascular space
Tissue signal intensity change	Darkening	Enhancement
Duration of effect and optimal data acquisition	Seconds; 1-2 s	Minutes; 2-25 s

Table 1. Comparison of dynamics MRI techniques [8].

However, other authors have defined DSC-MRI as a good technique to study tumor perfusion regardless of the location [36-39]; since some studies have shown that T2* effects are significantly stronger for intravascular contrast agents [40]. Nevertheless, other researchers have identified DCE-MRI as the optimal technique to study tumor

permeability, for the reason that T1 imaging is not affected by extravasation of the contrast agent. Whilst, DSC-MRI technique has as drawback the rapid loss of T2* imaging when the contrast agent extravasates in the interstitial space [41, 42].

Then with all this contradictory literature, it cannot be clarified which technique is better for DMRI [43-47]. Depending on the region of interest may be one is preferred according to the characteristics of each of the techniques. But in some situations literature has shown that both of them can be practiced (Figure 4) [8, 26, 45-47].

As an example of the possibility to employ both dynamic techniques to analyze a single region, a study developed in a patient with prostate cancer is presented in Figure 4.

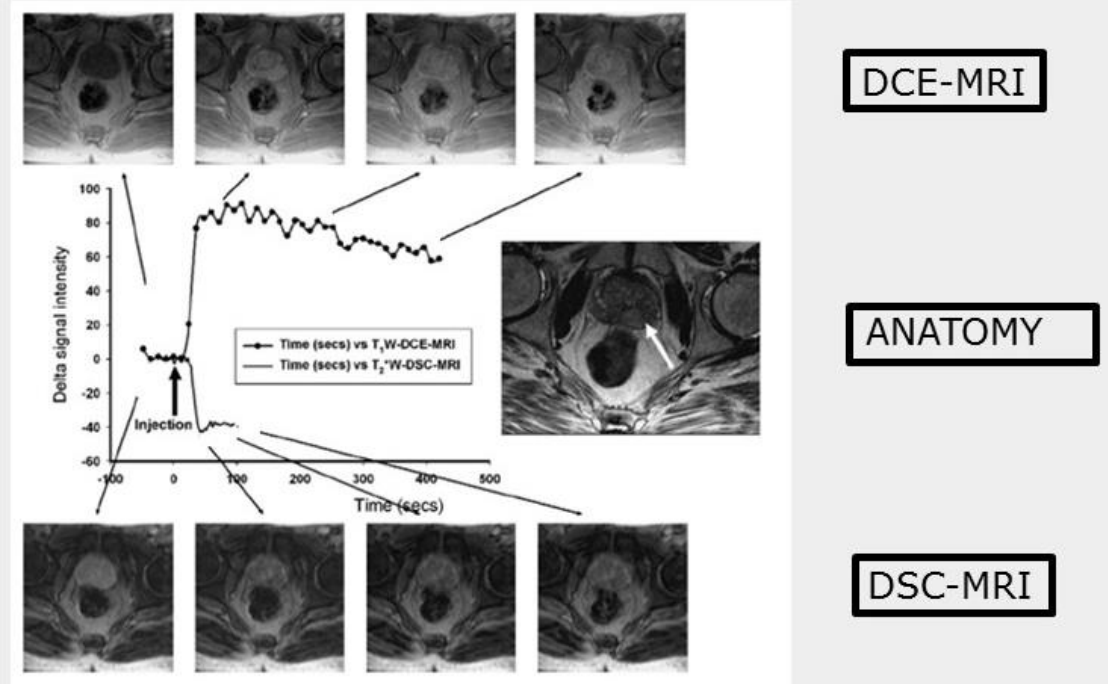

Figure 4. Comparison of the T1-weighted DCE-MRI (top) and T2-wieghted DSC-MRI (bottom) data collections from a patient with a prostate tumor, by the administration of Gd-DTPA [26].

Figure 4 shows a study where both DMRI imaging modalities have been tested. The white arrow of the image, located in the middle, point at the prostate tumor. Images situated at the top of the figure were obtained using DCE-MRI. Whilst, images located at the bottom of the figure were acquired using DSC-MRI. All images were obtained before, during and after contrast agent, as the black arrows of the graph indicate.

Focusing on the images obtained with DCE-MRI, it can be observed that as time passes after contrast agent administration the tumor becomes brighter. Nevertheless, in the images obtained with DSC-MRI occurs the other way around; with the pass of the contrast agent the tumor becomes darker [26].

So, since both methods can be practiced for studying tumor perfusion, and several literatures have differed in the use of one technique or other, both DMRI sequences will be evaluated in this project and the experimental setup/protocol for each of them will be optimized.

2.3 Data quantification

Signal intensity changes produced by the administration of a contrast agent, and the use of a DMRI sequence can be assessed qualitatively or quantitatively. Quantitatively they can be assessed by using pharmacokinetic model free variables or by the derivation of physiological indices using pharmacokinetic models [26].

Qualitative assessments are based on the shape of the TIC, and they are useful for tissue characterization and for assessing response to treatment [26].

Nevertheless, quantitative analysis aims to directly measure physiological parameters such as tissue blood flow, blood volume, interstitial volume or permeability-surface area. Depending on the DMRI sequence used for the images acquisition a different post-processing model will be employed.

2.3.1 DCE-MRI quantification

Multiple methods have been developed to analyze DCE-MRI data. Some of these methods are based on a model (model dependent), although others do not follow a defined model (non-model dependent). The use of these methods enables the knowledge of the pharmacokinetic parameters, which provide information on blood volume, blood

flow, microvessel permeability, contrast media concentration on EES, plasma and interstitium [24].

There are different approaches to analyze DCE-MRI images, such as Tofts, Hoffman, and Larsson [26, 48-52]. In this work data analysis was based on a model dependent method, Hoffman and on a non-model dependent, the curve parameters method will be carried out. Hoffman method is the second the pharmacokinetic model most widely applied to characterize murine tumors (the first one is Tofts models) [50]. And it was selected since it does not required pre-contrast and post-contrast map images for the analysis of the pharmacokinetic parameters [49], making the imaging protocol to be faster and simpler (because this method does not require T1 pre-contrast and post-contrast maps, as Tofts does).

Hoffman is a two-compartment model based on the linear relationship between MR signal enhancement and the contrast agent exchange rates. It is formed by a linear one-compartment model (central compartment) which represents the concentration of contrast media in the plasma; and a peripheral compartment connected to the central one by a linear exchange processes in both directions. This peripheral compartment represents the extracellular space of the tissue [48, 49].

According to the Hoffman model four different quantitative pharmacokinetic parameters can be calculated. The contrast agent infusion rate is determined by the constant K_{in}, which influences in the MR signal enhancement. However, the wash-out rate of the contrast is determined by other parameter, k_{el} (renal elimination constant). The remaining ones parameters k_{12} and k_{21} (also known as kep [26]) determine the diffusion rate of the contrast between the central compartment and the peripheral one; and vice versa. Figure 5 shows a schematic representation of Hoffman model.

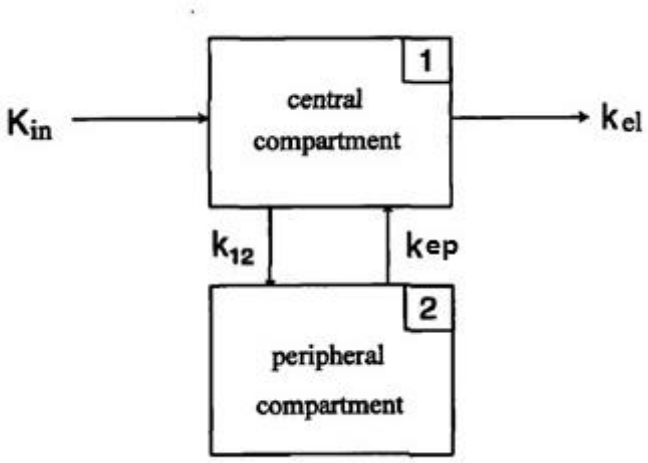

Figure 5. Schematic representation of the Hoffman model.

Mathematically this model can be described as

$$\frac{S(t)}{S_0} = 1 + A^H k_{ep} \left(\frac{e^{-k_{ep}t} - e^{-k_{el}t}}{k_{el} - k_{ep}} \right) \qquad (2.3)$$

where *S(t)* is the MR signal course while the contrast passes, S_0 is the MR signal before contrast agent injection and $A^H k_{ep}$ is considered an approximate measure of blood flow/perfusion of the tumor tissue (A^H approximately corresponds to the size of the EES) [50]. Thus, with these parameters and equation 2.3, it is possible to analyze the tumor perfusion.

The other method employed in this analysis, the curve parameters, is a model-free semi-quantitative analysis able to calculate three parameters. The initial area under the curve (IAUC) measures the amount of contrast delivered to and retained by the tumor in the given time period [53]. The relative contrast enhancement (RCE) defines those regions with higher contrast pass. And the last one is the time to maximum enhancement (TTM) of the contrast agent [50].

2.3.2 DSC-MRI quantification

The time-activity curve can be modeled by the contrast agent and the signal intensity of each pixel

$$S(t) = S_0 . e^{\frac{-C_m(t)}{k}} \qquad (2.4)$$

where *S(t)* is the time-activity curve (TAC) for a given pixel, S_0 is the baseline signal before the contrast agent arrival, $C_m(t)$ is the measured concentration of contrast agent as a function of time and k is a constant that depends on the scanner and the sequence used to acquire the image series.

By calculating the Arterial Input Function (AIF), which describes the signal intensity changes cause by the contrast agent in arteries near the region studied, the concentration of the contrast agent (as a function of time) and the idealized contrast bolus; three parametric maps can be calculated. The blood volume (BV), blood flow (BF) and the mean transit time (MTT).

The BV is defined as

$$BV = \frac{\int C_m(t)}{\int AIF\ (t)} \qquad (2.5)$$

The expression for MTT is

$$MTT = \frac{\int C(t)}{C_{max}} \qquad (2.6)$$

where *C(t)* is the pass of the contrast agent concentration without the effect of the circulatory system (idealized pass of the contrast agent), and C_{max} is the maximum of *C(t)* for that voxel.

Finally, these perfusion variables are related by the central volume theorem equation defining BF [24]

$$BF = BV/MTT \qquad (2.7)$$

Knowing all these parametric maps it is possible to study how vascularized and how perfused is the tumor. Regions bright in the BF maps are regions with high flux. Also, regions brighter in the BV map indicate a bigger amount of blood, which can be interpreted as higher vascularized regions.

Chapter 3

Materials and Methods

3.1 Animals

All animal procedures were approved by the Animal Experimentation Ethics Committee of Hospital General Universitario Gregorio Marañón (ES280790000087) and were performed according to EU directive (2010/63/UE) and national regulations (RD 53/2013). All animal manipulation processes have been developed by the co-director of the project Lorena Cussó Mula accredited with C category by the Comunidad de Madrid.

Three nude mice with subcutaneous xenograft of 215 pancreatic tumor located in the dorsal area, The 215 pancreatic tumors were obtained from patient's biopsies.

3.1.1 Animal preparation

Mice were anesthetized using 4% sevoflurane in oxygen at 1l/min. After being induced to anesthesia, they were placed in a supine position in the bed inside the MRI system, with the tumor region close to the coils that would be used for imaging (Figure 6B). Sevoflurane 1.5% in 100% oxygen at 3l/min was administered during MR scanning process (Figure 6A).

A) B)

Figure 6. Anesthesia system (A) and position of the mouse (B).

The depth of anaesthesia was monitored by the breathing rate (SA, Instruments). An intravenous catheter was inserted into the tail vein of each mouse for contrast agent administration. The catheter was connected with an injection line and linked to an injection pump (Figure 7A and 7B. Harvard Apparatus PHD 2000, programmable). Moreover, animal body temperature was maintained using a forced warm water system (Figure 7C. Gaymar) and monitored using a rectal temperature probe (Figure 7C. SA, Instruments).

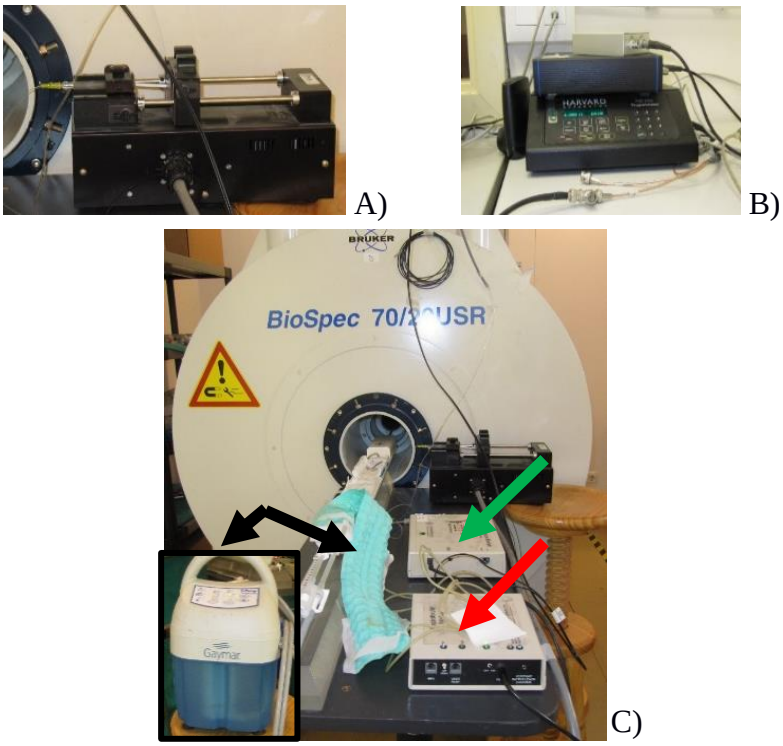

Figure 7. Instrumentation employed for the MR images acquisition. A) Injection pump. B) Programmable part of the injection pump. C) 7T MRI system where the black arrows point at the warm water system, the green at the rectal temperature motorization, and the red arrow point at the breathing rate monitor.

3.2 Image acquisition

MRI images were performed on a small animal 7T MRI system, using a volume coil for Tx and an abdominal phased-array coil, with four elements, in RX (BioSpec Bruker, Germany). As it has been exposed in Figure 7C.

For all dynamic images acquisition the order shown below was followed (Figure 8).

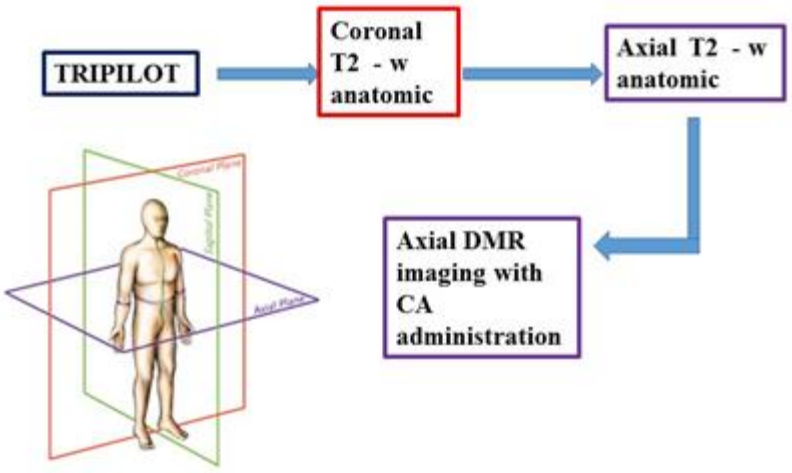

Figure 8. Diagram showing the imaging protocol for the DMRI images acquisition.

Figure 8 shows the general acquisition protocol for both DCE-MRI and DSC-MRI images. First of all, a Tripilot sequence was employed to position the mouse in the center of the scanner. Once the animal was placed, a coronal T2-w image was acquired to localize the tumor, followed by an axial T2-w sequence. T2-w sequences were selected due to its rapid image acquisition and good anatomical definition compared to the T1-w sequences. Once the axial image was acquired, the dynamic image was planned and performed with the contrast agent administration.

The parameters and sequences [31, 44, 45] employed in this project were selected after a carefully literature review [29, 31, 44, 45, 54-56]

The contrast agent selected to these studies was gadobutrol (Gadovist ®, Bayer Schering Pharma, Berlin, Germany) it is contrast media employer in clinical MRI researches that helps to discern healthy tissue from abnormal or injured tissue. To evaluate the optimal contrast agent concentration for the DCE-MRI acquisition two different contrast dilutions were tested. Firstly, the contrast agent Gadovist (1 mmol/ml) was used in a dose of 0.1 mmol/kg body weight, and diluted in a total volume of 0.2 ml. After it, the same image acquisition parameters were used but with a different contrast dose (0.05 mmol/kg body weight), and it was diluted in a total volume of 0.12 ml.

In DSC images acquisition also two contrast dilutions were tested to find the optimum one. However, in these experiments dose of Gadovist (1 mmol/ml) was maintained (0.5

mmol/kg body weight) and just the total volume (dilution) was changed. First, the total volume of contrast media of 0.2 ml, and then a volume of 0.12 ml.

3.2.1 DCE-MRI acquisition

For DCE-MRI studies the diagram showed in Figure 8 was followed. As mentioned, to evaluate the optimal contrast agent concentration for this sequence two different contrast dilutions of Gadovist were tested. Each of one was evaluated in a different animal, since two consecutive acquisitions cannot be performed because some time has to pass to eliminate the contrast agent residues.

For DCE-MRI images, a gradient-echo images were acquired using a Fast Low Angle Shot (FLASH) sequence and the following parameters: repetition time (TR) = 78ms, TE = 3.5 ms, matrix = 192x192, FoV = 2x4 mm, slice thickness = 1mm, number of averages (NA) = 1, number of slices= 8, number of repetitions= 100, and flip angle= 75º [44]. 8 images (temporal resolution: 23 s/image) were acquired before the administration of the contrast agent. Then, a bolus of 0.2 ml of Gadovist (0.1mmol/kg body weight) was injected with a constant rate of 0.2 ml/min [31]. Imaging time was 60 minutes.

Then, the same process was repeated in a different mouse maintaining all the DCE-MRI sequence parameters and changing the contrast dose: 0.05 mmol/kg body weight diluted in a volume of 0.12 ml.

3.2.2 DSC-MRI acquisition

As in the DCE-MRI, this dynamic imaging acquisition followed the diagram described in Figure 8. To obtain these DMRI images same contrast agent used in DCE-MRI was employed, in a dose of 0.5mmol/kg body weight [45]. To optimize the Gadovist concentration two contrast dilutions were tested too, and just the total volume (dilution) was changed from 0.2ml in the first experiment to 0.12 ml in the second one.. In these experiments both contrast dilutions were evaluated in the same mouse, but the images acquisition were performed in different days, since as it was mentioned before the body system needs some time to eliminate the contrast agent residues.

After the T2-w images in coronal and axial planes, a single slice of the axial image was selected (this technique requires a high temporal resolution due the rapid signal loss thus only one slice can be acquired) and the geometry adjusted. Then, the DSC-MRI images were acquired with a FLASH sequence. For it the following parameters were defined: TR= 5.44 ms, TE= 2.1 ms, flip angle= 15°, slice thickness= 1mm, number of repetitions= 300, matrix= 128x128, FoV= 2x4 mm, NA= 2, temporal resolution= 1 s/image. Before the contrast agent administration 30 images were acquired. After it, a bolus of 0.12 ml of Gadovist (0.5 mmol/kg body weight) was injected with a constant rate of 2.4 ml/min. The whole process time for acquiring DSC-MRI images was 40 minutes.

This process was redone with the same parameters in the same mouse (different day) just changing the total volume; now 0.2 ml administered, but maintaining the dose.

3.3 Image processing

Firstly, a qualitative analysis was executed to select the best protocol for each of the dynamic techniques; an ImageJ plugin (Dynamic Pixel Inspector) was employed to evaluate the quality of those images, this tool measured the intensity values per pixel in each image along time.

Once the best protocol was selected, the images were analyzed quantitatively (pharmacokinetic parameters and parametric maps). The images selected to evaluate with the programs were acquired from the same mouse, in different days (due to the reasons explained before). For their quantitative analysis two different softwares were used.

3.3.1 DCE-MRI analysis

To calculate the pharmacokinetic parameters many computer programs can be employed. But for the analysis of the data obtained in this project, the software application programmed in IDL, DCE@urLAB, developed in the Escuela Técnica Superior de Ingenieros de Telecomunicación (ETSIT) was used. It was selected due to its open source characteristic [50].

This tool is able to analyse a region of interest (ROI) within the image data by evaluating the contrast agent concentration in that ROI and its effect on T1 relaxation time and thus on pixel intensity.

This software application can analyse the images using five different pharmacokinetic models: Tofts [52], Hoffman [49], Larson, curve parameters and the reference region (RR) model. However, as mentioned before for simplicity just two of them were used for analysing DCE data: Hoffman and curve parameters models.

The process described in Figure 9 was followed in order to quantify the DCE-MRI images.

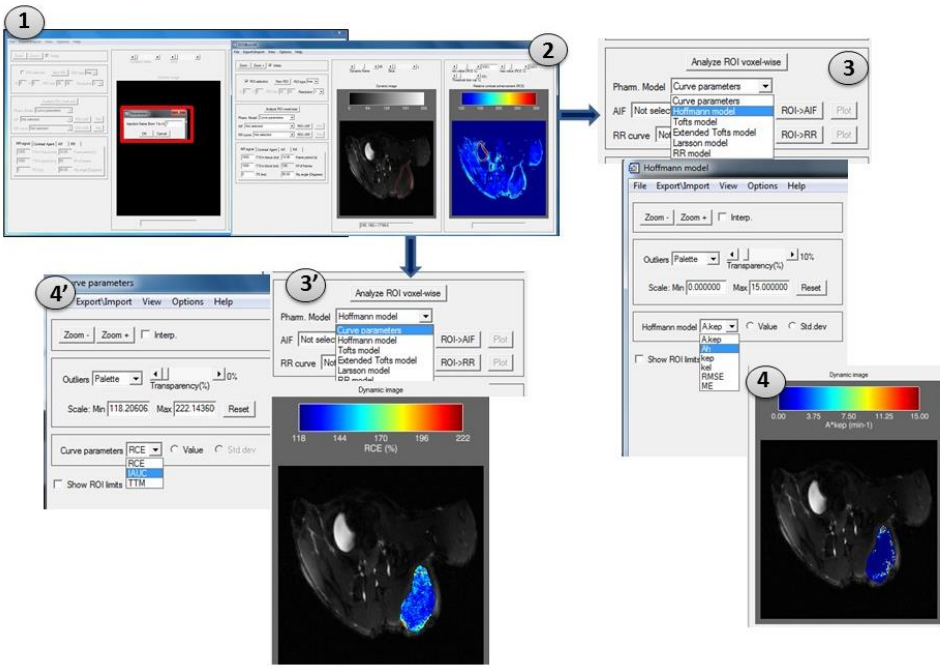

Figure 9. Process followed to quantify DCE images with DCE@urLAB software. Step 1 the software is opened, image imported and injection frame defined. Step 2 the ROI (tumor) is defined manually. Step 3 and 4 pharmacokinetic analysis of Hoffman model. Step 3' and 4' semi-quantitative analysis using the curve parameters model.

Firstly, the DCE-MRI images are imported to DCE@urLAB. After it, the injection frame is introduced (Figure 9 step 1). Two windows appear (Figure 9 step 2), the left one showing the original image (dynamic image); and the right one represents the image with a color code to indicate regions with higher contrast pass (RCE). See Figure 10. Then, a ROI (new ROI) is defined manually in the tumor region (Figure 9 step 2).

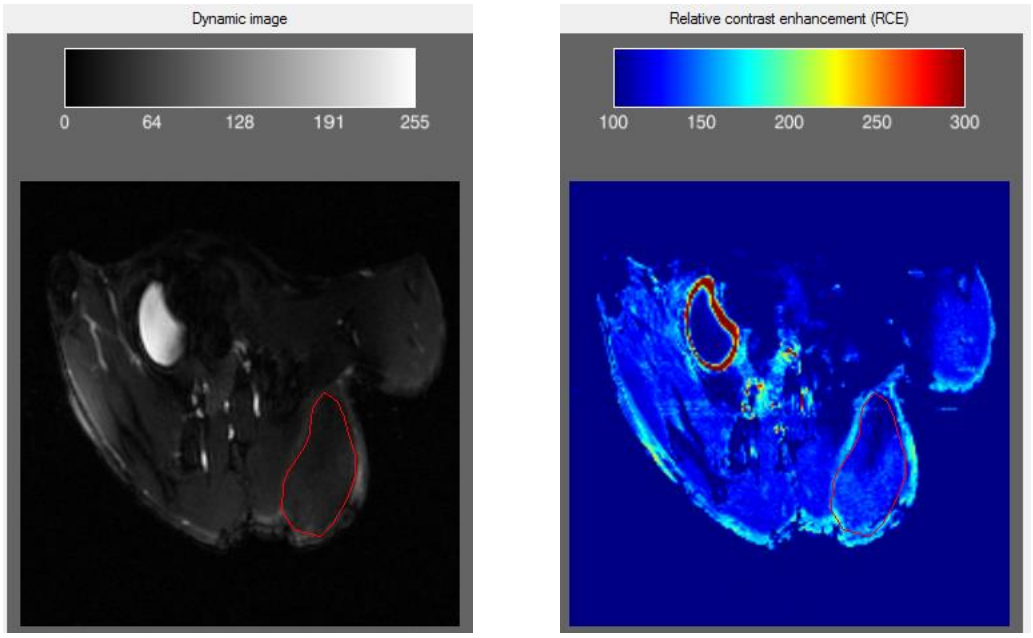

A) B)

Figure 10. Dynamic image (A) with a ROI defined, and relative contrast enhancement image (B) represented with DCE@urLAB software.

Once the ROI is defined, two pharmacokinetic methods are selected to analyze the image (Figure 9 step 3 and 3'). The curve parameters method and Hoffman model. This step (Figure 9 step 4 and 4') is repeated for each of the pharmacokinetic parameters (Hoffman: $A.k_{ep}$, A^{H}, k_{ep} and k_{el}; and Curve parameters: RCE, IAUC and TTM).

The scale bar can be adjusted for better tumor visualization (Figure 11).

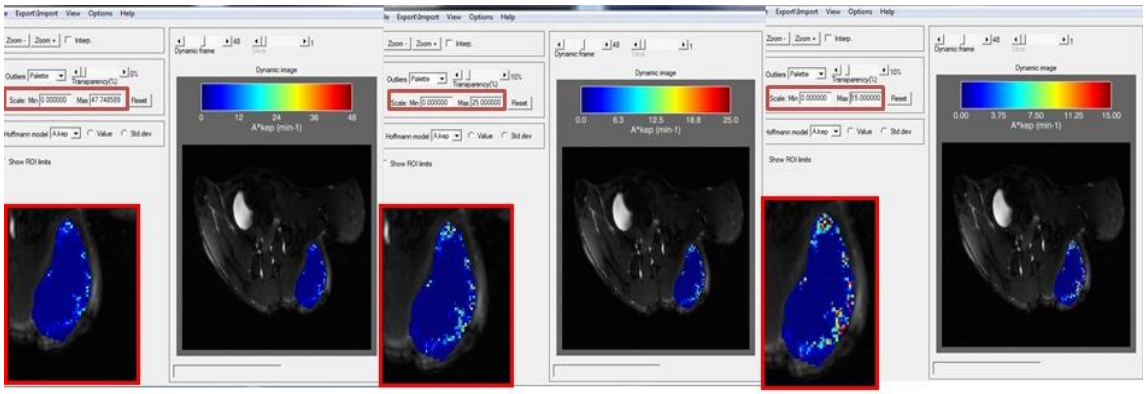

Figure 11. RCE images with different Min and Max values for the color scale.

3.3.2 DSC-MRI analysis

In the analysis of the set of images acquired by the DSC-MRI technique a plugin of open source characteristics of the ImageJ program was used, tool enable to analyse these images is LIMPERFUSION-1.0.0 [57]. For the visualization of the DSC-MRI parametric maps the software Multimodality WorkStation (MMWKS), developed in the Medical Imaging Laboratoryof the Hospital General Universitario Gregorio Marañón was used [58].

The process shown in Figure 12 was followed to analyze the whole image sets of DSC-MRI.

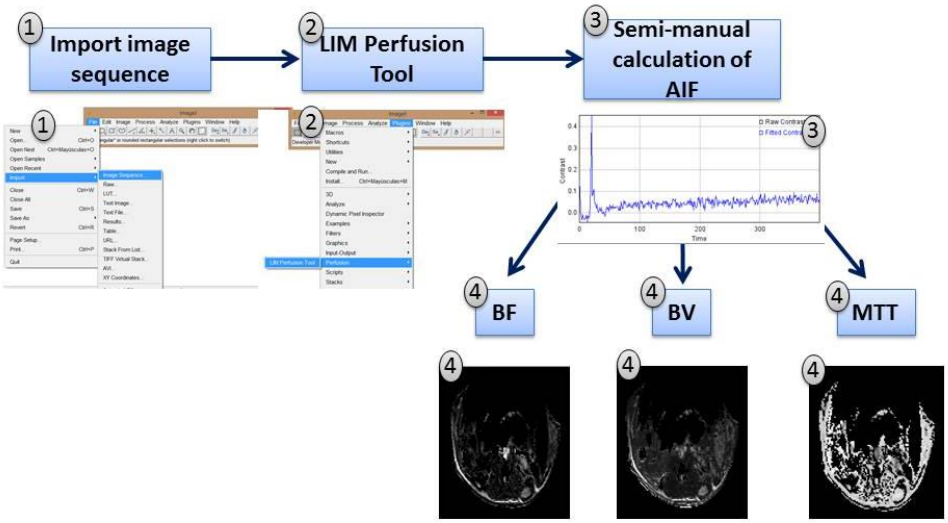

Figure 12. Order followed to analyze DSC-MRI data. Step 1 images imported to ImageJ. Step 2 LIM perfusion plugin is opened. Then, AIF is calculated semi-manually (step 3).Finally, parametric maps are obtained (step 4).

In order to remove undesired noise it is recommended to remove some frames at the beginning and at the end of the image set. Then, LIM Perfusion plugin is opened, and the AIF is selected manually (step 3 of Figure 12), by adding the points/pixels that show an AIF high and narrow, with an abrupt change (large, early, rapid intensity changes [45]; Figure 13). Once selected and accepted the three parametric maps are calculated: BV, BF and MTT (step 4 of Figure 12).

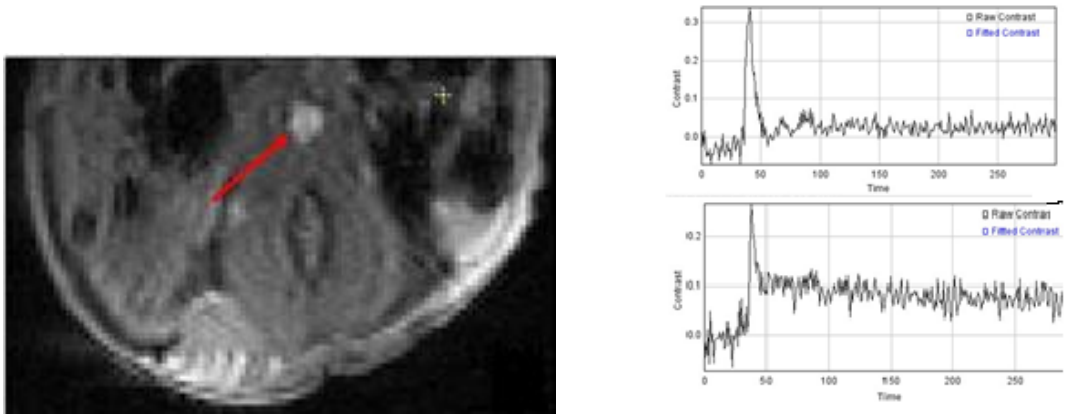

A) B)

Figure 13. Process to select a good AIF. A) Image analyzed, where the red arrow points at the aorta, region where the AIF should be selected. B) Top, example of a right AIF; bottom, example of a wrong AIF.

Chapter 4

Results

4.1 DCE-MRI optimization

The first image exposed in this section was acquired with the DCE protocol and a Gadovist dose of 0.1 mmol/kg diluted in a volume of 0.2 ml (Figure 14).

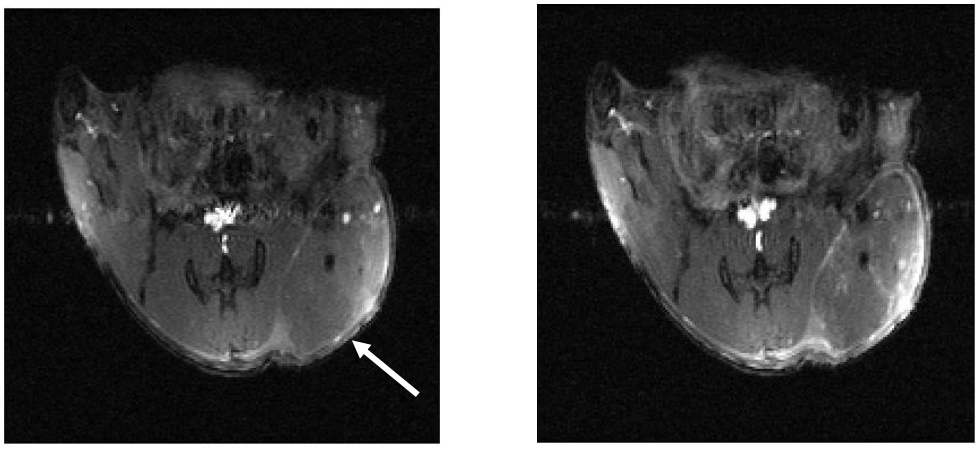

A) B)

Figure 14. DCE-MRI images acquired before (A) and after (B) the contrast agent administration; contrast dose and volume: 0.1 mmol/kg body weight in 0.2 ml. The white arrow points the tumor localization.

Figure 14 shows how the tumor becomes brighter once the contrast agent had been injected (Figure 14B). Before the contrast agent (Figure 14A) the tumor just is bright at its surroundings. While after the contrast media administration tumor becomes brighter at its surroundings but also inside it. Both images are shown with the same window-level.

These changes caused by the effect of the contrast agent in the relaxivity times of the tissues can also be seen with a color code bar in Figure 15. These images were represented using the Fire option of the ImageJ program, for a better appreciation of the intensity changes. In Figure 15B, it can be observed how the tumor becomes orange/yellow compared to Figure 15A. These changes in color represents the contrast pass and the effect caused by the DCE protocol, indicating the areas with more contrast pass (higher intensity value) orange/yellow, brighter; and the area with less contrast pass and enhancement blue/purple, those more darker (less intensity values).

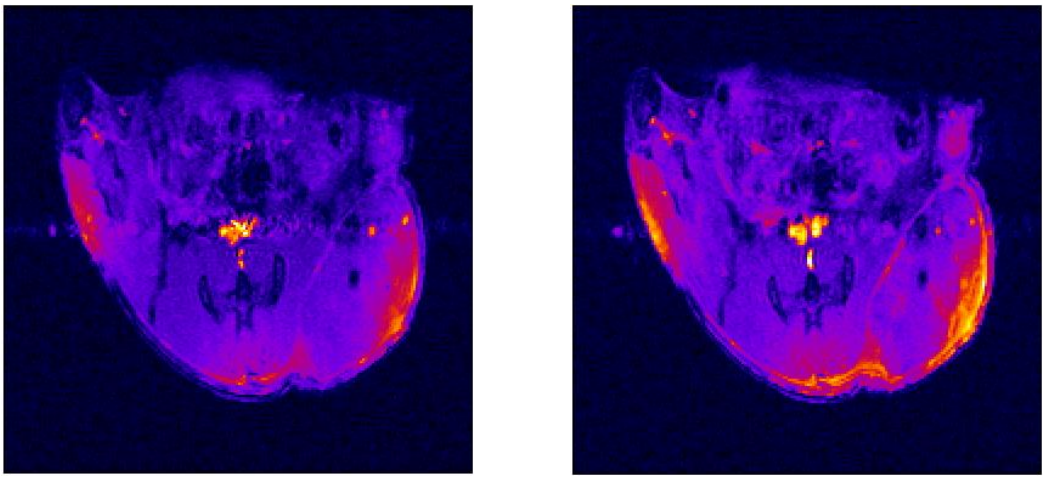

A) B)

Figure 15. DCE-MRI images acquired before (A) and after (B) the contrast agent administration using the Fire option of ImageJ, contrast dose and volume: 0.1 mmol/kg body weight in 0.2 ml.

The image quality was evaluated with the Dynamic Pixel Inspector plugin, and Figure 16 represents the results obtained. This plot indicates the intensity level of a selected pixel inside the tumor across time. It can be observed that after the injection of the contrast media intensity decreases (T2 effect), while it should increase due to the T1 effect of the contrast agent.

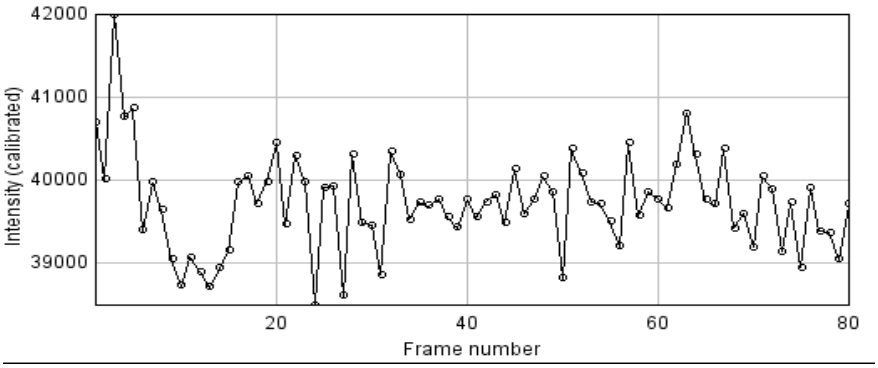

Figure 16. Dynamic Pixel Inspector analysis of DCE-MRI images with a Gadovist dose of 0.1 mmol/kg body weight diluted in 0.2 ml.

Images shown in Figure 17 were acquired using the same image protocol of Figure 14 (DCE image acquisition protocol) but in a different mouse, with different contrast dose and volume dilution (0.05 mmol/kg body weight and 0.12 ml respectively). Figure 17A was acquired before contrast agent injection and Figure 17 B, after it. It can be seen that in the tumor some changes occurred in the intensity (in the relaxivity of the tissues) during the contrast pass. Before the contrast administration the tumor presents a darker color while once the contrast agent passed, the tumor became brighter. Both images have the same window-level.

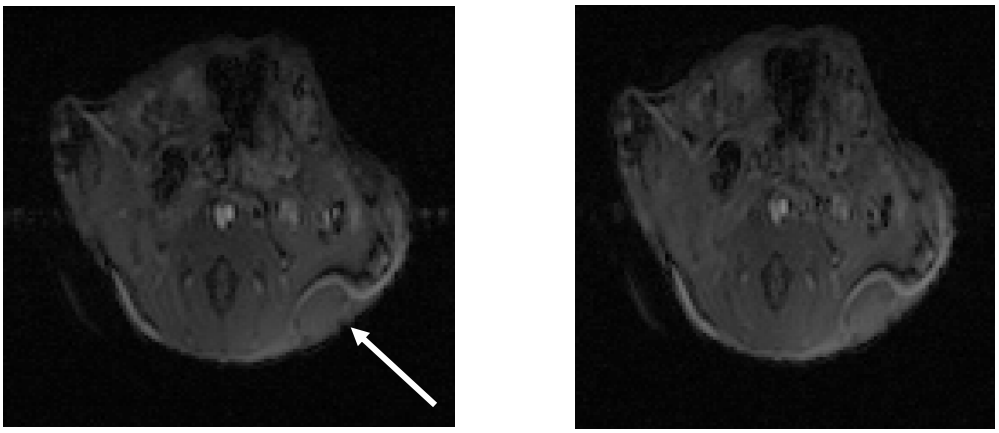

A) B)

Figure 17. DCE-MRI images acquired before (A) and after (B) the contrast agent administration; contrast dose and volume: 0.05 mmol/kg body weight in 0.12 ml. The white arrow points the tumor localization.

To visualize those changes easily, the Fire option of ImageJ was applied (Figure 18). Before the administration the tumor is represented with a purple tone, and after it the tumor is stained with a pinker color-scheme.

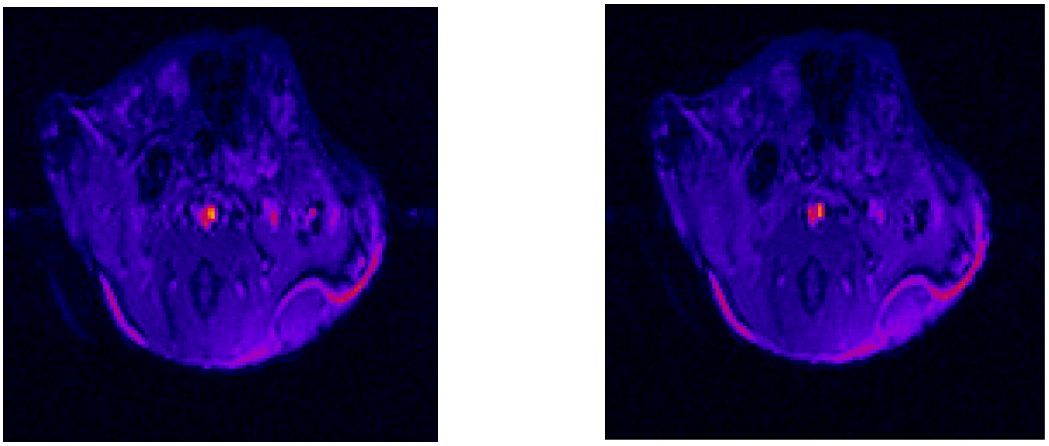

A) B)

Figure 18. DCE-MRI images acquired before (A) and after (B) the contrast agent administration using the Fire option of ImageJ. Gadovist dose 0.05 mmol/kg body weight, and diluted in 0.12 ml.

In Figure 19 it is presented the results obtained with the Dynamic Pixel Inspector tool in a region of the tumor. It was corroborated that after the contrast agent administration only T1 effect appeared in the tumor; the intensity values increased after the injection of the contrast media. Any T2 effect was noticeable.

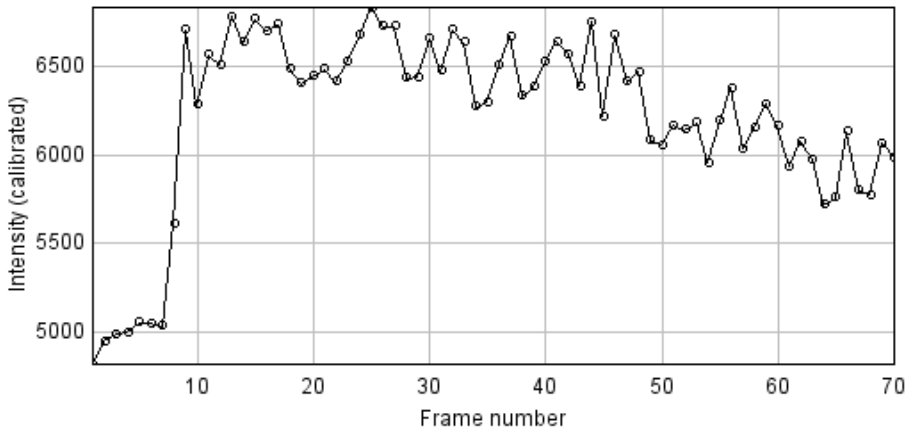

Figure 19. Dynamic Pixel Inspector analysis of DCE-MRI images with a Gadovist dose of 0.05 mmol/kg body weight diluted in 0.12 ml.

4.2 DSC-MRI optimization

Results obtained with the DSC image acquisition protocol are represented in the following figures. Figure 20 exposes the images acquired with the DSC-MRI protocol and a contrast volume of 0.12 ml.

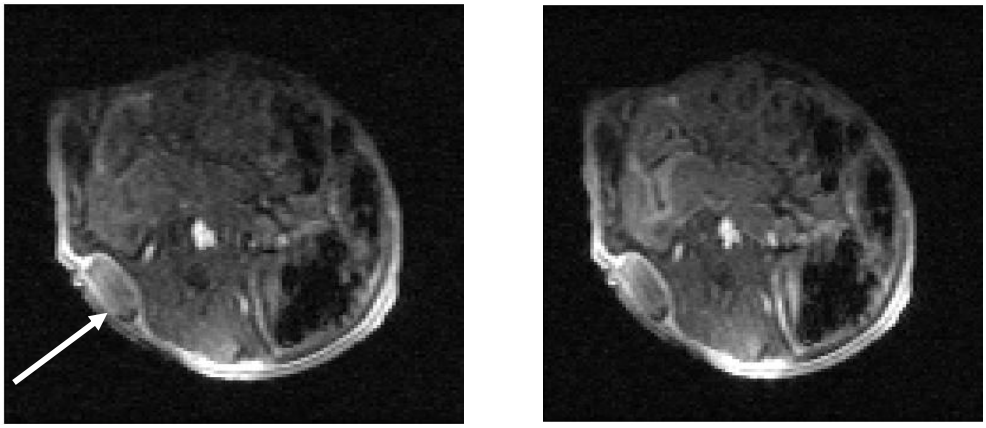

A) B)

Figure 20. DSC-MRI images acquired before (A) and after (B) the contrast agent administration; contrast agent volume 0.12 ml. The white arrow points the tumor localization.

In Figure 20 it can be observed that the tumor does not show significant changes in intensity before and after the contrast agent administration (both images have the same window-level.). As in the rest of the images, the Fire option was applied in these images to observe contrast enhancement with a different color code (Figure 21).

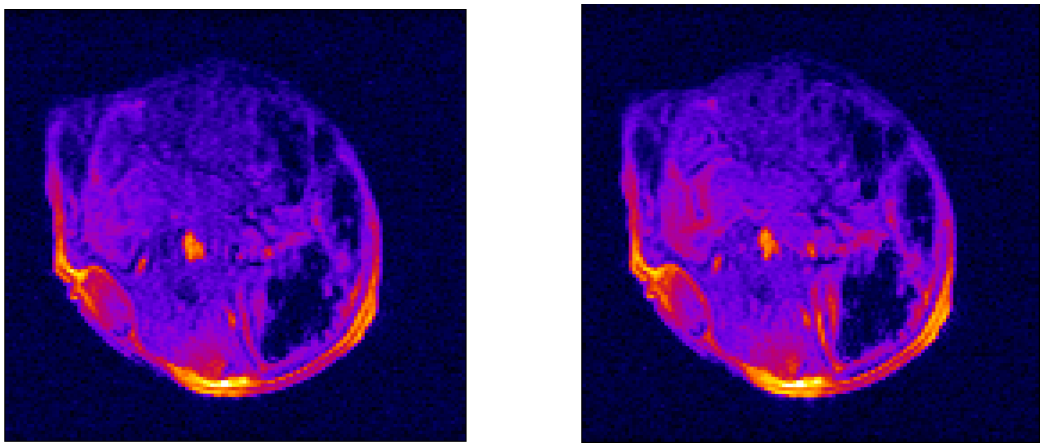

A) B)

Figure 21. DSC-MRI images acquired before (pre-contrast image; A) and after (post-contrast image; B) the contrast agent administration using the Fire option of ImageJ. Contrast agent volume 0.12 ml.

As in Figure 20, no relevant changes in the color-scheme of the tumor are observed. This lack of change was confirmed by using the Dynamic Pixel Inspector plugin (Figure 22).

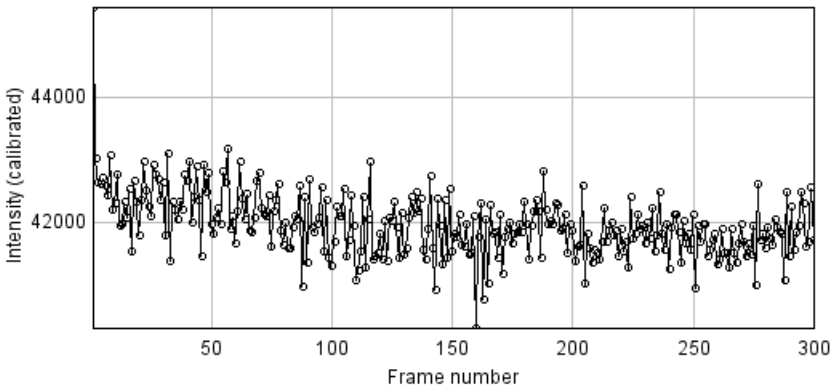

Figure 22. Dynamic Pixel Inspector analysis of DSC-MRI images with a contrast media of 0.12 ml

The next set of images (Figure 23 represents the DSC images acquired with the same protocol as in Figure 20, but with a different contrast agent volume (0.2 ml). It can be observed how the intensity levels changed after the administration of the contrast agent. By looking at the tumor region, it can be seen that before the contrast injection the tumor was brighter. Whilst, when the contrast was injected the tumor became darker. This darkening was caused by the changes in the relaxivity times of the tissues, which provoked a decreased in the intensity levels.

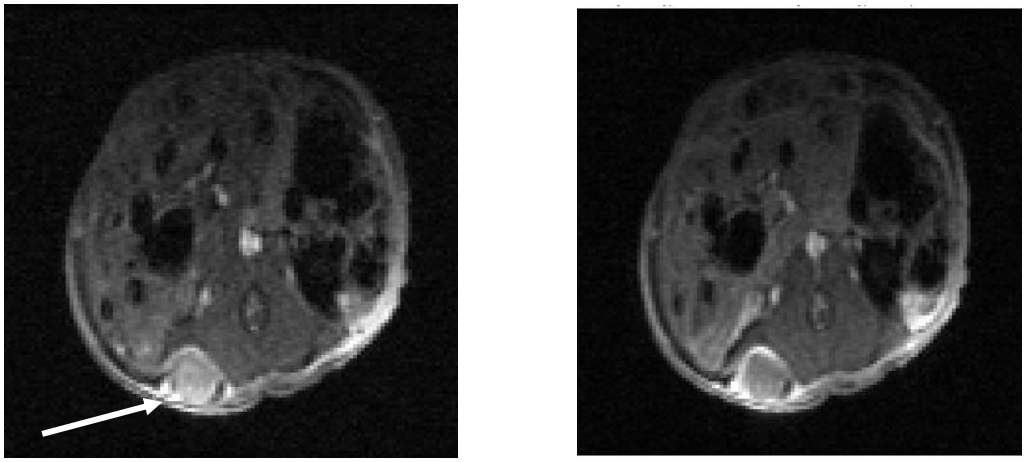

A) B)

Figure 23. DSC-MRI images acquired before (pre-contrast image; A) and after (post-contrast image; B) the contrast agent administration; contrast agent volume 0.2 ml. The white arrow points the tumor localization.

Both images have the same window-level (Figure 23). As in the rest of images, the Fire option was applied to observe these contrast changes with a color code (Figure 24). It can be observed contrast agent affects to the intensity levels changing from an orange/yellow color-scheme to a pink/purple tone.

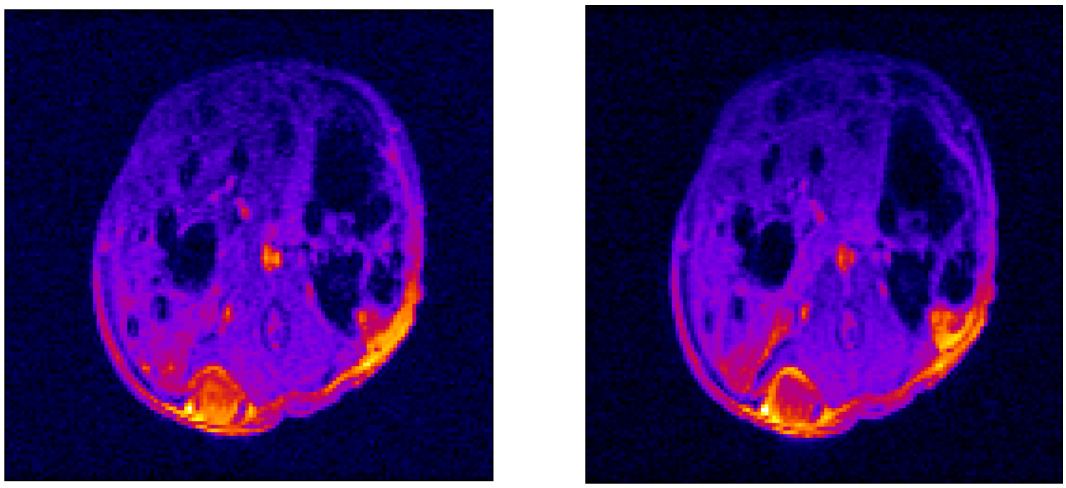

A) B)

Figure 24. DSC-MRI images acquired before (pre-contrast image; A) and after (post-contrast image; B) the contrast agent administration using the Fire option of ImageJ. Contrast agent volume 0.2 ml.

This darkening is confirmed by the used of the Dynamic Pixel Inspector plugin, Figure 25

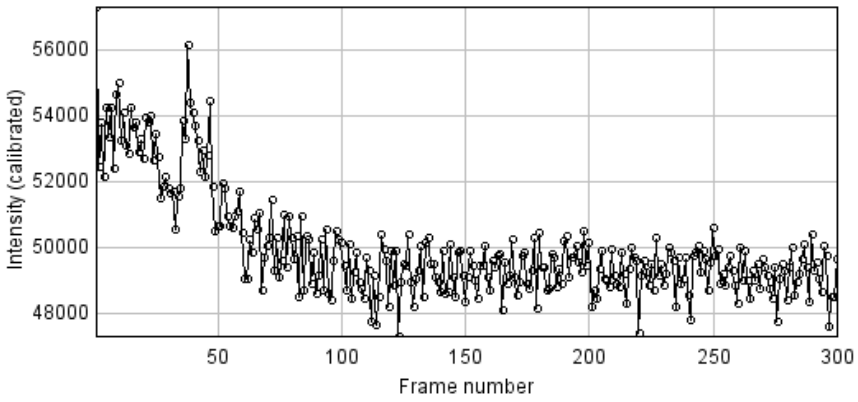

Figure 25. Dynamic Pixel Inspector analysis of DSC-MRI images with a contrast media of 0.2 ml

4.3 Quantitative analysis

In the previous section it was seen that only one of the protocols in each case gave optimal results. These optimized protocols were (DCE and DSC) analyzed quantitatively using the quantification methods explained before (Section 3.3 Image processing). As it was mentioned, in this case, the images compared were obtained from the same mouse in different days which explains the different tumor locations in the images.

4.3.1 DCE-MRI quantification

Images acquired with the only successful DCE-MRI protocol (0.05 mmol/kg body weight diluted in 0.12 ml) were analysed with the DCE@urLAB program following the processes defined in Figure 9. As the figure shows, two different methods were employed in this analysis (curve parameters and Hoffman model).

Figure 26 presents the original image with the tumor selected as the ROI, where parameters were calculated.

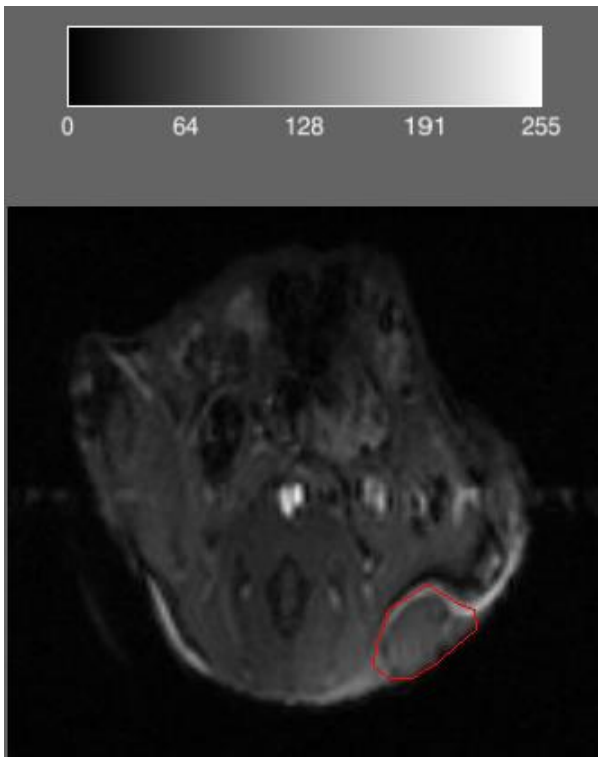

Figure 26. Original DCE-MRI image with the ROI selected for the quantification analysis.

In the next set of images (Figure 27) the pharmacokinetic parameters (A.k_{ep}, A^H, k_{ep} and k_{el}) obtained using the Hoffman model are exposed. All the images present each own color-scale with their maximum and minimum values.

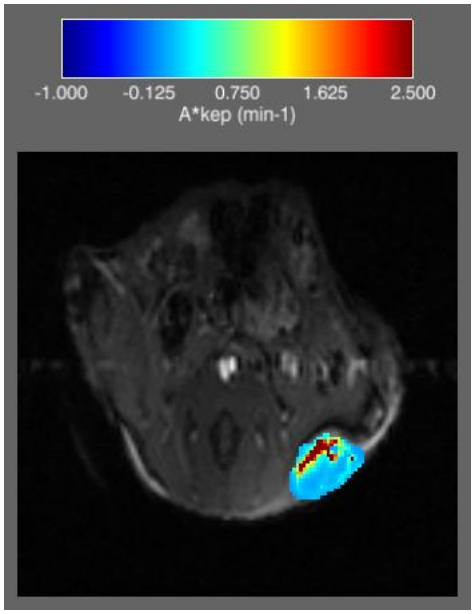

A)

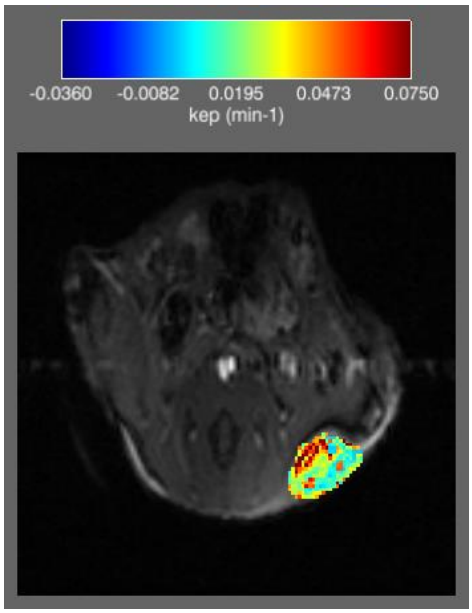

B)

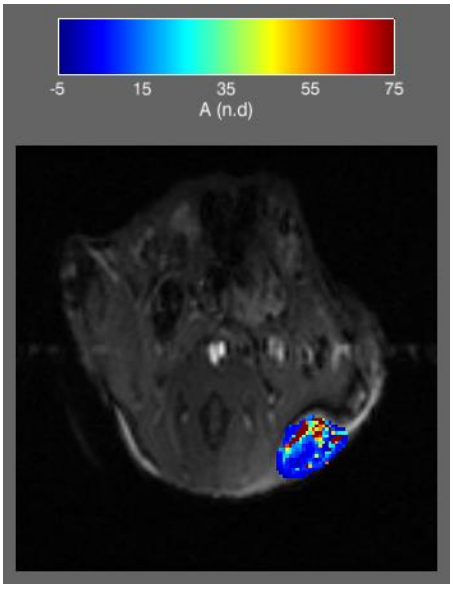

C)

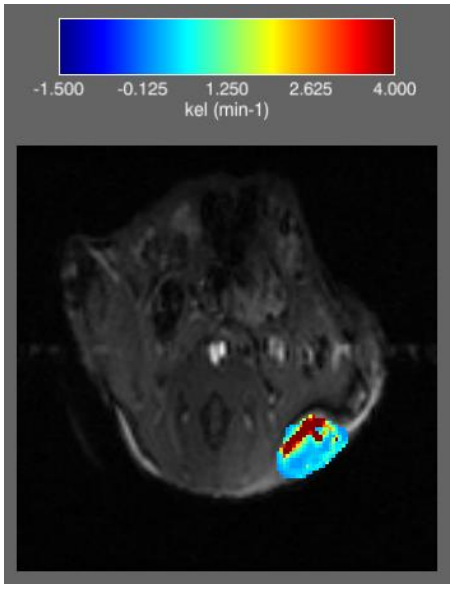

D)

Figure 27. Pharmacokinetic parameters of the Hoffman model in the ROI (tumor) of DCE-MRI images. A) A.kep; B) kep; C) A^H; and D) kel

In Figure 27A Ak_{ep} measured in min^{-1} can be observed, where the higher values (according to the color-scheme bar) of this constant are at the left-top region of the tumor. Thus, this region is characterized by its higher values of blood flow/perfusion. Figure 27B exposed the different values of k_{ep} (unit min^{-1}) parameter of the ROI, in general there are medium values (between 0.02-0.04), and the higher ones can be find in the surroundings of the upper part of the tumor and some of them in the center. Figure 27C displays the A^H (size of the EES) parameter, which presents higher values in the left zone of the ROI (according to the color-scheme bar). Finally, Figure 27D represents the k_{el} (min^{-1}, elimination rate of the contrast agent), and it can be seen that the left-top region shows higher elimination rate (around 50 min^{-1}).

The results obtained in the analysis of the curve parameters model (IAUC, RCE and TTM) are shown in Figure 28. The IAUC parameter is shown in Figure 28A, in general, the whole tumor presents high values (higher ones, close to 5, at the top-left of the ROI) of IAUC. The same occurs with the RCE parameter, in Figure 28B it can be seen that the whole tumor has high values of RCE (between 100 and150). This indicates that the whole tumor is a region with high contrast enhancement. Finally, Figure 28C shows the TTM of the tumor, indicating the bottom of the ROI as a region with high values.

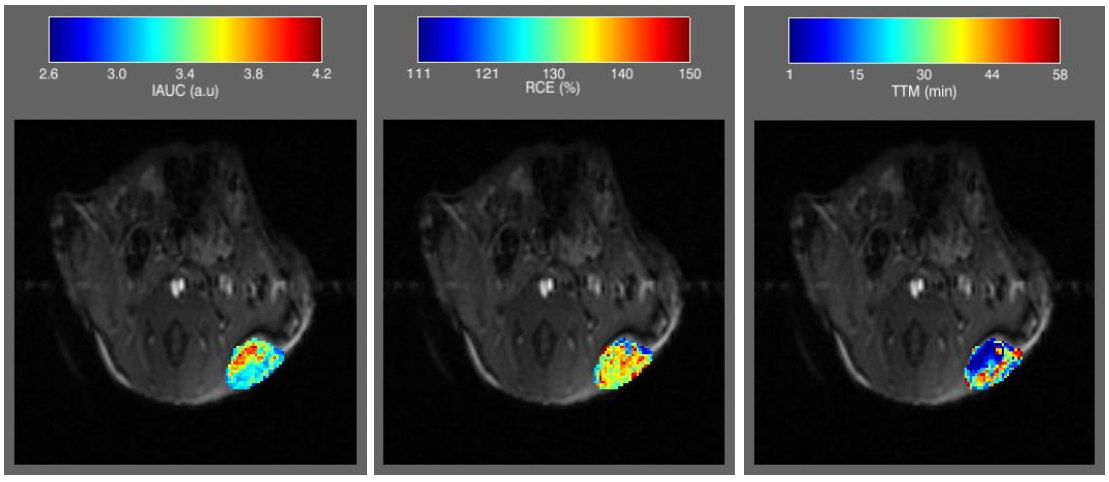

A) B) C)

Figure 28. Parameters of the curve parameters model in the ROI (tumor) of DCE-MRI images. A) IAUC; B) RCE; and C) TTM.

4.3.2 DSC-MRI quantification

The DSC protocol selected with one of the contrast volume (0.2 ml of contrast media) was analysed with the LIMPERFUSION- 1.0.0 plugin of the ImageJ program. Three parametric maps were obtained for each dynamic image: BV, BF and MTT.

Figure 29 shows two DSC images acquired before (Figure 29A) and after (Figure 29B) the contrast agent administration. In both of them it the intensity changes (decrease in the intensity values) in the tumor region (located at the bottom- right area of the image) occasioned by the contrast media can be observed.

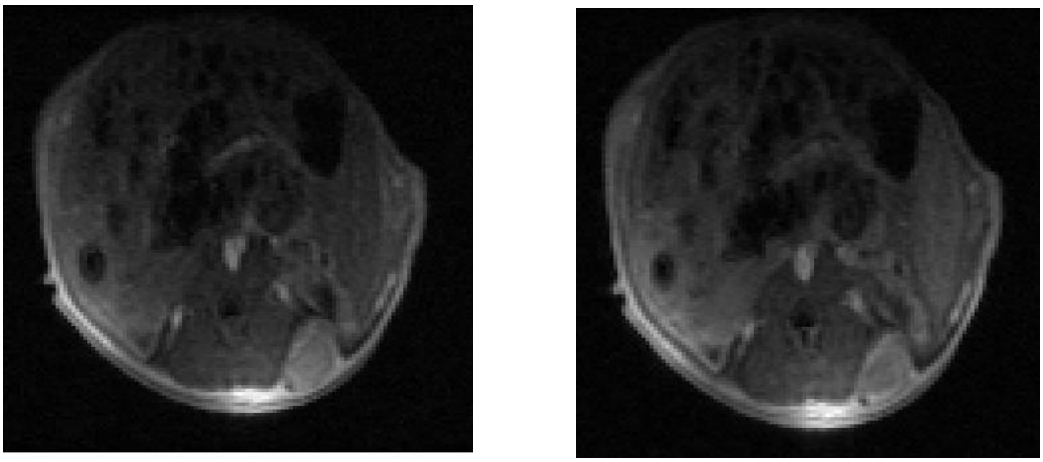

A) B)

Figure 29. DSC-MRI images acquired before (pre-contrast image; A) and after (post-contrast image; B) the contrast agent administration; contrast agent volume 0.2 ml.

Figure 30 represents the BV parametric map. Where Figure 30A represents the BV map in the original scale (grays) and the other one presents the same image with a red-blue color scheme obtained with the MMWKS program, Figure 30B. In all the images of Figure 30 it can be observed the regions with higher BV, according to the different color-schemes used. Figure 30A shows brighter the tumor region, which means that inside of the tumor is a higher BV value compared with the rest of the tumor Figure 30B shows the same results in the different color scale, a yellow/orange tone (values between 0.57-1.48).

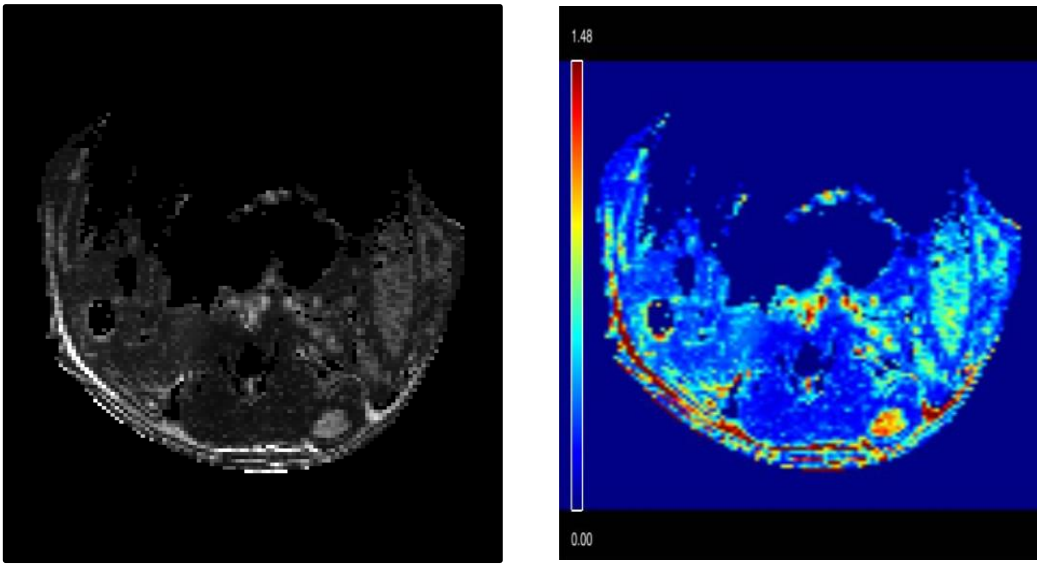

A) B)

Figure 30. BV parametric map represented in two color scales. A) Grays. B) MMWKS program (red-blue color scheme).

Figure 31 defines the BF parametric map, where the areas with higher BF are represented brighter (gray levels, Figure 31A), yellow/orange (red-blue color scheme obtained in the MMWKS program, Figure 31B).

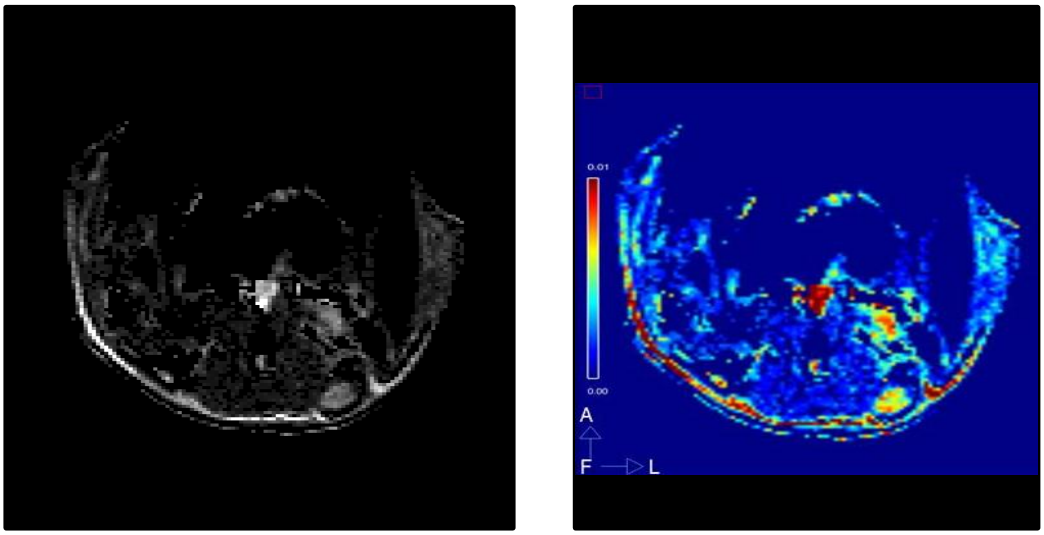

A) B)

Figure 31. BF parametric map represented in different color scales. A) Grays. B) MMWKS program (red-blue color scheme).

In the following image (Figure 32) the MTT parametric map is shown. In the image, the areas more homogenized are the areas with similar MTT value, which means areas with similar BV/BF ratio. These similar values can be corroborated looking at Figure 30 and Figure 31.

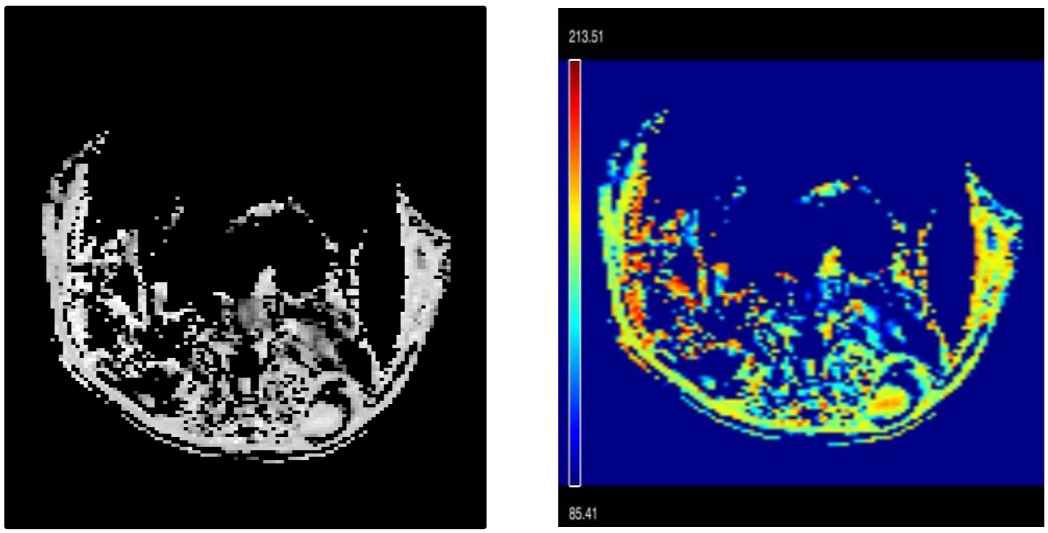

A) B)

Figure 32. MTT parametric map represented in the gray scale (A), and in the red-blue color scheme acquired with the MMWKS (B).

Chapter 5
Discussion

In this project two protocols for dynamic imaging acquisition to analyze pancreatic tumor perfusion in mice have been optimized, one for DCE-MRI and the other one for DSC-MRI.

As it was mentioned before, the image protocol was selected based on the literature [31, 44, 45]. To optimize the DCE-MRI protocol two different contrast doses of Gadovist were tested in two different mice: 0.1 mmol/kg body weight diluted in 0.2 ml in one mouse, and 0.05 mmol/kg body weight diluted in 0.12 ml in the other mouse. While the optimization of DSC-MRI protocol was achieved by testing two different contrast media volumes (keeping constant the Gadovist dosage): 0.2 and 0.12 ml in the same mouse, but not in consecutive acquisitions.

Once the protocols with proper behavior were assessed, Gadovist dilution 0.05 mmol/kg in 0.12 ml for DCE-MRI and Gadovist 0.5 mmol/kg diluted in 0.2 ml for DSC-MRI, the dynamic images were analyzed with DCE@urLAB and LIMPERFUSION 1.0.0 programs. Pharmacokinetic parameters of DCE-MRI and parametric maps of DSC-MRI enable the knowledge of the tumor perfusions, concretely Ak_{ep} and BV [46, 50].

5.1 DCE-MRI optimization

Results obtained with both contrast agent administration rates, shown in Figure 14 and Figure 17, have demonstrated that the optimal contrast dose and volume was 0.05 mmol/kg body weight and 0.12 ml respectively.

In the case of the 0.1 mmol/kg dose, despite some brightening can be observed after the administration of the contrast agent, the results obtained with the Dynamic Pixel Inspector plugin (Figure 16) indicated some T2 effects in the image, since the intensity values decayed after the contrast agent administration. So this dose was discarded.

Some authors have mentioned that the contribution of T2 effects can be minimized by using a more diluted contrast agent solution [34]. This was confirmed with the results obtained by lowering the dose (0.05 mmol/kg body weight diluted in 0.12 ml). The results obtained with this Gadovist dose (Figure 17) indicate a brightening of the tumor region after the contrast passed. Moreover, the intensity-frame graph (Figure 19) acquired with the Dynamic Pixel Inspector demonstrates that the contrast agent has not effect on T2 relaxivity values.

So, results have verified that the protocol selected for DCE-MRI images acquisition with a 0.05 mmol/kg body weight diluted in 0.12 ml was optimal to study pancreatic tumor

5.2 DSC-MRI optimization

Two different protocols for the optimization of DSC-MRI image acquisition were tested (Figure 20 and Figure 23 shows the results obtained). As in the DCE-MRI experiments, the MRI parameters were maintained in both analysis, but contrast agent volume was changed (keeping constant the dose of Gadovist). The two contrast agent volume (0.2 ml and 0.12 ml) indicated different results in the pre and post-contrast images. Just the contrast volume of 0.2 ml showed intensity values changes after the contrast pass (Figure 23).

No intensity changes were observed after the contrast injection Figure 22 for the first volume tested. This indicates that maybe a bolus of that volume is not enough to reach the tumor region or to perfuse it. Maybe a higher volume is required to perfuse the tumor region and to be "captured" by the coil of the MR system.

Therefore, the results obtained in the 0.2 ml contrast media have verified the optimal protocol for the acquisition of DSC-MRI images, and thus for its analysis (parametric maps BV, BF and MTT) to study pancreatic tumor perfusion (Figure 30, Figure 31 and Figure 32).

5.3 DCE and DSC: comparative

Images obtained (belonging to the same mouse) with the protocols selected explained before were analysed. DCE-MRI images were analysed with the software application DCE@urLAB. And DSC-MRI parametric maps were calculated using the ImageJ plugin LIMPERFUSION 1.0.0.

The quantification and the results obtained with both programs have demonstrated that both protocols have been successfully optimized, and also it has been verified that a proper analysis of those can be achieved.

In this project, DCE images were assessed by analysing the TIC (curve parameters method, semi-quantitative and non-model dependent) and by quantifying the contrast agent concentration changes using the pharmacokinetic model technique. Semi-quantitative parameters were calculated due their simplicity of calculus. However, this analysis (curve parameters) presents some limitations like the inability to accurately reflect contrast agent concentration in the tissue of interest (tumor), can be influenced by scanner settings and do not directly inform on tissue physiology [8, 26]. So, to overpass these limitations quantitative parameters are analysed. In this project Hoffman model was selected because of its simplicity and high temporal resolution compared to other models (it does not require pre and post T1-w maps as Tofts model requires).

The quantification analysis of the DSC-MRI images was developed to inform about tumor perfusion, since as was mentioned DSC-MRI technique is sensitive to the

presence of the contrast within the vascular space [24]. However, it should be mentioned that the information obtained with DSC quantification methods is relative, since absolute quantification of the DSC data is not currently possible. Thus, tracer kinetic principles can be used to provide estimates of relative blood volume (rBV), relative blood flow (rBF) and MTT [8].

The differentiation of both DMRI techniques, such as the temporal resolution, the compartments studied and the complexity affects to the information obtained with each of them [8, 26]. In the case of DCE-MRI, the temporal resolution is lower (2-25 seconds), then the contrast can be tracked in a longer term; and the compartments studied are two (EES and intravascular). Then, it can be said that the parameters acquired with this quantification are more related with tumor permeability information; concretely, the Ak_{ep} pharmacokinetic parameter [50]) (Figure 27). Nevertheless, the characteristics of DSC-MRI technique (high temporal resolution, intravascular space studied, etc.) enable to provide information about the tumor perfusion (BV, BF and MTT parametric maps, Figure 30, Figure 31 and Figure 32 [24]).

To determine the accuracy of the results obtained with DCE-MRI and DSC-MRI, and to evaluate if the information obtained from them is complementary or equivalent, histological proofs are required. Histological proofs would corroborate if the regions higher permeable coincide with the regions with higher k_{ep} value, and the same with the regions higher perfused and BV and BF parameters. Moreover, it would be determined the relation of DCE and DSC parameters, if permeable regions correspond to perfused regions. Finally, if both protocols were equivalent a single technique could be used to study tumor perfusion. Under this hypothesis the DSC-MRI protocol would be preferred due to its higher temporal resolution and its simpler process (compared to the DCE one) [8, 26].

Chapter 6
Conclusions and future perspectives

6.1 Conclusions

In this work, two different approaches (DCE-MRI and DSC-MRI) to study the perfusion grade of subcutaneous 215 pancreatic tumors were tested and compared. MRI sequences and contrast doses were selected after a carefully review of the literature.

For the optimization of DCE-MRI protocol two mice were used, in each of them a different dose was tested. Results obtained with the Dynamic Pixel Inspector plugin has established 0.05 mmol/kg body weight as the optimal contrast agent dose, and 0.12 ml as the optimal contrast media volume for the acquisition of a DCE image with high resolution, and without any contrast agent effects in T2 relaxivity time of the tissues.

In the evaluation of DSC-MRI protocols, the same mouse was used in different acquisition days with two different concentrations of the contrast agent Results obtained with Dynamic Pixel Inspector plugin have determined 0.2 ml as the optimal contrast bolus volume for the acquisition of high resolution DSC images.

Once the optimal protocols and their doses were determined, each of them was tested in the same mouse, with a day of difference to clean the contrast agent residues. Then,

images acquired with both approaches were analyzed. DCE data has been analyzed with the non-model dependent method curve parameters, and quantify with the Hoffman model; both analyzed with the DCE@urLAB program [50]. DSC images have been analyzed with the LIMPERFUSION 1.0.0 software [57]. Both protocols were successfully analyzed and the results obtained provide good indicators of tumor perfusion [46, 50].

6.2 Future perspectives

There exists a wide range of future approaches to continue with this project.

As it was mentioned before, a histology analysis could be highly advantageous to compare and evaluate both DMRI techniques. The quantitative parameters obtained with both techniques give information about the morphology of tumors, indicating those regions higher vascularized and those more necrotic; this information would be confirmed or disproved based on histological studies.

Another approach would be to evaluate the DCE quantification with other model. Hoffman model was selected because of its simplicity. However, this model could have some limitations, since the information obtained about the tumor physiology is less specific than the one obtained with other methods; as for example the Tofts model; which is the most widely used in measuring vessel permeability [24]. Tofts model requires the acquisition of pre-contrast and post-contrast T1 maps. If the data required for both Hoffman and Tofts is acquired and both models analysed, the histology data would be also useful to evaluate the advantages and disadvantages of each model [49, 52].

References

1. Available from: http://emice.nci.nih.gov/aam.
2. Morales Pérez, J.M., et al., *Resonancia magnética dinámica en el diagnóstico de las lesiones tumorales y seudotumorales del sistema musculoesquelético.* TITLEREVISTA, 2012. **54**(Supl.1): p. 38-49.
3. Desco, M. and J.J. Vaquero, *Imagen molecular en medicina.* 2007.
4. Desco, M. and J.J. Vaquero, *Imagen Molecular.* Profesión Veterinaria, 2009. **año 16, nº 70** (Diciembre 2008-Marzo 2009): p. 68-76.
5. Pysz, M.A., S.S. Gambhir, and J.K. Willmann, *Molecular imaging: current status and emerging strategies.* Clin Radiol, 2010. **65**(7): p. 500-16.
6. Estorch, M. and I. Carrio, *Future Challenges of Multimodality Imaging*, in *Molecular Imaging in Oncology*, O. Schober and B. Riemann, Editors. 2013, Springer Berlin Heidelberg. p. 403-415.
7. Benjaminsen, I.C., et al., *Assessment of tumor blood perfusion by high-resolution dynamic contrast-enhanced MRI: A preclinical study of human melanoma xenografts.* Magnetic resonance in medicine, 2004. **52**(2): p. 269-276.
8. Jeswani, T. and A.R. Padhani, *Imaging tumour angiogenesis.* Cancer Imaging, 2005. **5**(1): p. 131.
9. Systems, P.M., *Principles of MR Imaging*. 1984: Philips, Medical Systems.
10. Desco, M. and J.J. Vaquero, *Más de un siglo de imagen médica [More than a century of medical imaging]*. Arbor - Ciencia pensamiento y cultura, 2004. **CLXXVII**(698): p. 337-364.

11. Brown, M.A. and R.C. Semelka, *Concepts of Magnetic Resonance*, in *MRI*. 2005, John Wiley & Sons, Inc. p. 11-19.
12. Brown, M.A. and R.C. Semelka, *Frontmatter*, in *MRI*. 2005, John Wiley & Sons, Inc. p. i-xiv.
13. Brown, M.A. and R.C. Semelka, *Principles of Magnetic Resonance Imaging—Part 1*, in *MRI*. 2005, John Wiley & Sons, Inc. p. 33-47.
14. Brown, M.A. and R.C. Semelka, *Principles of Magnetic Resonance Imaging—Part 2*, in *MRI*. 2005, John Wiley & Sons, Inc. p. 49-65.
15. Brown, M.A. and R.C. Semelka, *Pulse Sequences*, in *MRI*. 2005, John Wiley & Sons, Inc. p. 67-91.
16. Brown, M.A. and R.C. Semelka, *Relaxation*, in *MRI*. 2005, John Wiley & Sons, Inc. p. 21-31.
17. Levitt, M.H., *Spin dynamics: basics of nuclear magnetic resonance*. 2008: John Wiley & Sons.
18. Yankeelov, T.E., et al., *Repeatability of a reference region model for analysis of murine DCE-MRI data at 7T.* Journal of Magnetic Resonance Imaging, 2006. **24**(5): p. 1140-1147.
19. Verstraete, K.L., et al., *Benign and malignant musculoskeletal lesions: dynamic contrast-enhanced MR imaging--parametric "first-pass" images depict tissue vascularization and perfusion.* Radiology, 1994. **192**(3): p. 835-43.
20. Brown, M.A. and R.C. Semelka, *Contrast Agents*, in *MRI*. 2005, John Wiley & Sons, Inc. p. 213-222.
21. Bjørnerud, A., *The physics of magnetic resonance imaging. Kompendium for FYS-KJM 4740*. 2008: Universitetet i Osio.
22. Weinmann, H.J., et al., *Characteristics of gadolinium-DTPA complex: a potential NMR contrast agent.* American Journal of Roentgenology, 1984. **142**(3): p. 619-624.
23. Bokacheva, L., et al., *High-field small animal magnetic resonance oncology studies.* Physics in Medicine and Biology, 2014. **59**(2): p. R65.
24. Li, S.P. and A.R. Padhani, *Tumor response assessments with diffusion and perfusion MRI.* Journal of Magnetic Resonance Imaging, 2012. **35**(4): p. 745-763.
25. Daldrup, H.E., et al., *Quantification of the extraction fraction for gadopentetate across breast cancer capillaries.* Magn Reson Med, 1998. **40**(4): p. 537-43.

26. Alonzi, R., A.R. Padhani, and C. Allen, *Dynamic contrast enhanced MRI in prostate cancer.* European journal of radiology, 2007. **63**(3): p. 335-350.
27. van Dijke, C.F., et al., *Mammary carcinoma model: correlation of macromolecular contrast-enhanced MR imaging characterizations of tumor microvasculature and histologic capillary density.* Radiology, 1996. **198**(3): p. 813-818.
28. Hormigo, A., P.H. Gutin, and S. Rafii, *Tracking normalization of brain tumor vasculature by magnetic imaging and proangiogenic biomarkers.* Cancer cell, 2007. **11**(1): p. 6-8.
29. Barnes, S.L., et al., *Assessing the reproducibility of dynamic contrast enhanced magnetic resonance imaging in a murine model of breast cancer.* Magnetic Resonance in Medicine, 2013. **69**(6): p. 1721-1734.
30. Jensen, L.R., et al., *Assessment of early docetaxel response in an experimental model of human breast cancer using DCE-MRI, ex vivo HR MAS, and in vivo1H MRS.* NMR in biomedicine, 2010. **23**(1): p. 56-65.
31. Partecke, I.L., et al., *In vivo imaging of pancreatic tumours and liver metastases using 7 Tesla MRI in a murine orthotopic pancreatic cancer model and a liver metastases model.* BMC cancer, 2011. **11**(1): p. 40.
32. Quarles, C.C., et al., *Functional colonography of Min mice using dark lumen dynamic contrast-enhanced MRI.* Magnetic Resonance in Medicine, 2008. **60**(3): p. 718-726.
33. Farrar, C.T., et al., *In vivo validation of MRI vessel caliber index measurement methods with intravital optical microscopy in a U87 mouse brain tumor model.* Neuro-oncology, 2010. **12**(4): p. 341-350.
34. Zhou, H., M. Chen, and D. Zhao, *Longitudinal MRI Evaluation of Intracranial Development and Vascular Characteristics of Breast Cancer Brain Metastases in a Mouse Model.* PloS one, 2013. **8**(4): p. e62238.
35. Griebel, J., et al., *Assessment of tumor microcirculation: a new role of dynamic contrast MR imaging.* Journal of Magnetic Resonance Imaging, 1997. **7**(1): p. 111-119.
36. Aumann, S., et al., *Quantification of renal perfusion using an intravascular contrast agent (part 1): Results in a canine model.* Magnetic Resonance in Medicine, 2003. **49**(2): p. 276-287.

37. Kuhl, C.K., et al., *Breast neoplasms: T2* susceptibility-contrast, first-pass perfusion MR imaging.* Radiology, 1997. **202**(1): p. 87-95.
38. Morell, A., et al., *Quantitative renal cortical perfusion in human subjects with magnetic resonance imaging using iron-oxide nanoparticles: influence of t1 shortening.* Acta Radiologica, 2008. **49**(8): p. 955-962.
39. Rosen, B.R., et al., *Perfusion imaging with NMR contrast agents.* Magnetic Resonance in Medicine, 1990. **14**(2): p. 249-265.
40. Villringer, A., et al., *Dynamic imaging with lanthanide chelates in normal brain: contrast due to magnetic susceptibility effects.* Magn Reson Med, 1988. **6**(2): p. 164-74.
41. Boxerman, J.L., K.M. Schmainda, and R.M. Weisskoff, *Relative Cerebral Blood Volume Maps Corrected for Contrast Agent Extravasation Significantly Correlate with Glioma Tumor Grade, Whereas Uncorrected Maps Do Not.* American Journal of Neuroradiology, 2006. **27**(4): p. 859-867.
42. Calamante, F. and F. Calamante, *Artifacts and pitfalls in perfusion MR imaging Clinical MR Neuroimaging*. 2009: Cambridge University Press.
43. Gambarota, G., et al., *Characterisation of tumour vasculature in mouse brain by USPIO contrast-enhanced MRI.* British journal of cancer, 2008. **98**(11): p. 1784-1789.
44. Guntle, G.P., et al., *Tumor xenograft response to redox-active therapies assessed by Magnetic Resonance Imaging using a thiol-bearing DOTA complex of gadolinium.* Translational oncology, 2012. **5**(3): p. 190.
45. Pike, M., et al., *High-resolution longitudinal assessment of flow and permeability in mouse glioma vasculature: Sequential small molecule and SPIO dynamic contrast agent MRI.* Magnetic Resonance in Medicine, 2009. **61**(3): p. 615-625.
46. Muldoon, L.L., et al., *Dynamic magnetic resonance imaging assessment of vascular targeting agent effects in rat intracerebral tumor models.* Neuro-oncology, 2011. **13**(1): p. 51-60.
47. Varallyay, C.G., et al., *Dynamic MRI using iron oxide nanoparticles to assess early vascular effects of antiangiogenic versus corticosteroid treatment in a glioma model.* Journal of Cerebral Blood Flow & Metabolism, 2009. **29**(4): p. 853-860.

48. Cho, H., et al., *Noninvasive multimodality imaging of the tumor microenvironment: registered dynamic magnetic resonance imaging and positron emission tomography studies of a preclinical tumor model of tumor hypoxia.* Neoplasia (New York, NY), 2009. **11**(3): p. 247.
49. Hoffmann U, B.G., Knopp MV, Hess T, Lorenz WJ, *Pharmacokinetic mapping of the breast - a new method for dynamicMR mammography.* . Magn ResonMed, 1995. **33**: p. 506–514
50. Ortuno, J.E., et al., *DCE@urLAB: a dynamic contrast-enhanced MRI pharmacokinetic analysis tool for preclinical data.* BMC Bioinformatics, 2013. **14**: p. 316.
51. Tofts, P.S., et al., *Estimating kinetic parameters from dynamic contrast-enhanced t1-weighted MRI of a diffusable tracer: Standardized quantities and symbols.* Journal of Magnetic Resonance Imaging, 1999. **10**(3): p. 223-232.
52. Tofts, P.S. and A.G. Kermode, *Measurement of the blood-brain barrier permeability and leakage space using dynamic MR imaging. 1. Fundamental concepts.* Magnetic Resonance in Medicine, 1991. **17**(2): p. 357-367.
53. Walker-Samuel, S., M. Leach, and D. Collins, *Evaluation of response to treatment using DCE-MRI: the relationship between initial area under the gadolinium curve (IAUGC) and quantitative pharmacokinetic analysis.* Physics in medicine and biology, 2006. **51**(14): p. 3593.
54. Hartono, S., et al. *High temporal resolution dynamic contrast-enhanced MRI at 7 Tesla: A feasibility study with mouse liver model*. in *Engineering in Medicine and Biology Society, EMBC, 2011 Annual International Conference of the IEEE*. 2011. IEEE.
55. Loveless, M.E., et al., *A quantitative comparison of the influence of individual versus population-derived vascular input functions on dynamic contrast enhanced-MRI in small animals.* Magnetic Resonance in Medicine, 2012. **67**(1): p. 226-236.
56. Smith, D.S., et al., *Quantitative effects of using compressed sensing in dynamic contrast enhanced MRI.* Physics in medicine and biology, 2011. **56**(15): p. 4933.
57. Macías Gordaliza, P., *Implementación de una herramienta para medidas de perfusión cerebral en imagen de resonancia magnética bajo ImageJ*, in *Departamento de Bioingeniería e Ingeniería Aeroespacial. Escuela Politécnica*

Superior, J.M. Mateos and J.J. Vaquero, Editors. 2013, Universidad Carlos III de Madrid.

58. Pascau, J., et al., *Multimodality workstation for small animal image visualization and analysis.* 2006.